Multiproxy reconstruction of oceanographic conditions in the southern epeiric Kupferschiefer Sea (Late Permian) based on redox-sensitive trace elements, molybdenum isotopes and biomarkers

Wolfgang Ruebsam[a,*], Alexander J. Dickson[b], Eva-Maria Hoyer[a] and Lorenz Schwark[a,c,*]

[a] *Department of Organic Geochemistry, University of Kiel, Germany*

[b] *Department of Earth Sciences, University of Oxford, Oxford, UK*

[c] *WA-OIGC, Curtin University, Perth, Australia*

*Corresponding authors.

E-mail address: wr@gpi.uni-kiel.de (Wolfgang Ruebsam); ls@gpi.uni-kiel.de (Lorenz Schwark)

ABSTRACT

The key drivers controlling the redox state of seawater and sediment pore waters in low energy environments can be inferred from redox-sensitive trace elements (RSTE), molecular biomarkers and trace metal isotopes. Here, we apply a combination these tools to the Upper Permian Kupferschiefer (T1) from the Thuringian Basin, deposited in the southern part of the semi-enclosed Kupferschiefer Sea. Enrichment patterns of the RSTEs molybdenum (Mo) and uranium (U) as well as biomarker data attest to the rapid development of euxinic conditions in basin settings during early T1 times, which became progressively less extreme during T1 deposition. The evolution of redox conditions in basinal settings, and the associated delay in the onset of euxinia at more shallow marginal sites, can be attributed to the interaction of sea-level change with basin paleogeography. Euxinia in the southern Kupferschiefer Sea did not lead to near-quantitative depletion of aqueous Mo, possibly due to short deepwater renewal times in the Thuringian Basin, low aqueous H_2S concentrations, the continuous resupply of RSTE during

transgression and declining burial rates of RSTEs throughout T1 times. Drawdown of RSTE is, however, indicated for euxinic lagoon environments. Moreover, admixture of freshwater supplied to these lagoons by rivers strongly impacted on local seawater chemistry. The highest Mo-isotope compositions of ~1.70‰ in basin sediments allows a minimum Kupferschiefer Sea seawater composition of ~2.40‰ to be estimated. This composition is similar to the ~2.30‰ estimate for the Late Permian open ocean, and confirms a strong hydrographic connection between the epeiric Kupferschiefer Sea and the global ocean. The substantial variation in Mo-isotope signatures is paralleled by diagnostic shifts in biomarkers responding to oxygenation in different parts of the water column. Water column chemistry has been affected by variation in sea level, hydrodynamic restriction, riverine freshwater influx and evaporitic conditions in shallow lagoons. Elucidation of the relative role of each driving factor by a single geochemical proxy is not feasible but the complex scenario can be disentangled by a multiproxy approach.

keywords: *euxinic basins, photic zone euxinia, basin restriction, element drawdown, freshwater influx*

1. Introduction

The paleoceanographic and paleodepositional conditions in ancient marine environments will control or be controlled by biotic community structures, organismic evolution including mass extinction, nutrient and other element fluxes mainly via the influence of the redox potential in pore, deep and surface waters. The reconstruction of oceanographic conditions, including redox state as well as hydrology, can be achieved through measuring the abundance and distribution of redox-sensitive trace elements (RSTE) in sedimentary deposits, as well as the isotopic compositions of many of these elements (e.g. molybdenum). In sediments that experienced only minor diagenetic thermal overprint, the molecular composition of organic matter (biomarkers) can provide highly detailed information on redox conditions in the pore water and the water column. The most detailed and comprehensive information on ancient environmental conditions can, however, be obtained from the combined application of these semi-independent techniques.

Enrichment patterns of uranium (U) and molybdenum (Mo) have been widely applied to characterize the redox regime of marine systems (e.g. Emerson & Huested, 1991; Crusius et al., 1996; Tribovillard et al., 2006, 2012; Algeo & Tribovillard, 2009; Dickson and Cohen, 2012), which can be classified as oxic (> 2.0 ml O_2/l); suboxic (0.2 – 2.0 ml O_2/l), anoxic (<0.2 ml O_2/l) or euxinic (presence of free H_2S) (e.g. Wignall, 1994). Moreover, enrichment pattern of U and Mo in combination with the abundance of organic matter (OM) can provide information on seawater chemistry, deep water renewal times and, thus, on the hydrological regime (Algeo & Lyons, 2006; Algeo & Rowe, 2012). U and Mo are present in seawater as $UO_2(CO_3)_3^{4-}$ and MoO_4^{2-}species, respectively. Under reducing conditions, dissolved U(VI) species are reduced to insoluble UO_2, U_3O_7, or U_3O_8 (IV), whose deposition occurs across the sediment-water interface (Algeo & Tribovillard, 2009 and references therein). Mo-removal from the water column requires the formation of (oxy)thiomolybdates ($MoO_xS_{4-x}^{2-}$, x = 1-4), which occurs in the presence of aqueous H_2S (Helz et al., 1996; Erickson & Helz, 2000; Helz et al., 2011). The redox potential required for Mo-uptake is lower than for U-uptake. Therefore, enhanced U uptake relative to Mo occurs under suboxic-anoxic conditions, whereas Mo removal rates from seawater exceed those of U under anoxic-euxinic conditions (Algeo & Tribovillard, 2009). In euxinic semi-enclosed basins, hydrogeographic factors such as deep water renewal times can further impact on trace element accumulation rates, as the aqueous trace element inventory declines if the rate of removal from seawater exceeds that of resupply (e.g. Algeo & Lyons, 2006; Algeo & Rowe, 2012).

The Mo-isotope composition of sediments ($\delta^{98/95}Mo_{SED}$, where $\delta^{98/95}Mo = ({}^{98/95}Mo_{sample} - {}^{98/95}Mo_{NIST\ 3134})/{}^{98/95}Mo_{NIST\ 3134}$ x 1000) is governed by the variable mixing of sulfide and oxide sedimentary phases, which exhibit different degrees of isotopic fractionation from seawater (Siebert et al., 2003, 2006; Poulson et al., 2006; Poulson-Brucker et al., 2009, 2012). In oxic waters slow Mo-removal via adsorption onto Mn-oxides is associated with a fractionation of -3‰ (Barling & Anbar, 2004), whereas in suboxic-anoxic waters Mo-adsorption onto Fe oxyhydroxides is associated with variable fractionation of -0.8 to -2.2‰ relative to seawater (Goldberg et al., 2009). Mo is bound to sulfides in sulfidic water masses and pore waters with a smaller fractionation of -0.5 to -0.9‰ relative to seawater (Siebert et al., 2003, 2006; Poulson-Brucker et al., 2009, 2012; Neubert et al., 2008; Nägler et al., 2011). Where aqueous H_2S concentrations exceed 11µmol/l, near-quantitative Mo-depletion in the water column causes the

basin seawater $\delta^{98/95}$Mo to increase (Nägler et al., 2011), which is tracked by the sedimentary $\delta^{98/95}$Mo until the latter approximates the global seawater $\delta^{98/95}$Mo outside the basin, as observed in the Black Sea. Therefore, the sedimentary Mo-isotope signature of euxinic sediments can provide information on the isotopic composition of the seawater that can be associated with changes in Mo fluxes (input/output) and the extent of oxic versus euxinic sinks (Barling et al., 2001; Arnold et al., 2004).

Biomarker proxies build on the preservation of biomolecules from organisms thriving in different habitats under various environmental conditions (e.g. salinity, nutrient supply, temperature, light penetration, oxygen availability and presence of toxic hydrogen disulfide in either pore, deep or surface waters). Many of these biomarkers are thermally labile and disappear at burial temperatures of less than 80-100°C. Unlike RSTEs, redox-controlled biomarker proxies are not affected by reservoir effects and therefore provide hydrologically independent information on the redox regime. The distribution pattern of prokaryote-derived C_{31} to C_{35} hopanes varies as a function of redox conditions (Peters et al., 2005 and references therein), whereby C_{35} hopanes are preserved under preferentially euxinic conditions via sulfurisation reactions (Sinninghe Damsté et al., 1995). Moreover, the availability of reduced sulfur for incorporation into OM can be assessed by the ratio of dibenzothiophene to phenanthrene (DBT/Phen) (Hughes et al., 1995). The presence of H_2S in the photic zone, termed photic zone euxinia (PZE), can be inferred from the occurrence of isorenieratane, diagnostic for the presence of *Chlorobiaceae*, which are green sulfur bacteria that perform anoxygenic photosynthesis (see Summons & Powell (1986) and review by Sinninghe Damsté & Schouten (2006)).

Here we apply a combination of these proxies to the Permian Kupferschiefer (Wuchiapingian; ~256 Ma BP; Stollhofen et al., 2008; Schurlies, 2013; Ogg et al., 2016) from the Thuringian Basin, a bituminous clay- or marlstone, deposited under anoxic-euxinic conditions in a semi-enclosed intracontinental basin with a narrow connection to the global ocean (Fig. 1a) (Wedepohl, 1971; Vaughan et al., 1989; Grice et al., 1997; Peryt et al., 2010). The multiproxy approach allows redox- and hydrologically-induced processes to be inferred, and a depositional model to be constructed. In the case of the marginal sub-basins of the Permian Kupferschiefer Sea in Thuringia, the low thermal maturity of the sediments allows to cross-validate RSTE and Mo isotopes against various biomarker proxies and thus to identify driving forces other than redox conditions that may impact on RSTE and Mo isotope proxies.

2. Geological setting, paleogeography and sequence stratigraphy

The Kupferschiefer Sea was established by catastrophic flooding of the Permian intracontinental depression, situated below sea level on the northern foreland of the Variscan Orogen (Ziegler, 1990; Gast et al., 2010). Flooding of this depression formed an epeiric semi-enclosed sea with an area of about 600,000 km^2 (Wedepohl, 1971). It was caused by a eustatic sea level rise, in combination with rifting between Laurentia and Eurasia that established a marine corridor between the Arctic Ocean and the European Permian Basins via the Norwegian-Greenland Sea (e.g. Glennie & Buller, 1983; Pharaoh et al., 2010). Inundation of the Permian intra-continental basins led to intensive reworking and leaching of uppermost Rotliegend clastics to form the so-called Weissliegend clastics or Zechstein conglomerate (Z1C), directly underlying the Kupferschiefer (Gast et al., 2010; Paul, 2006).

The Kupferschiefer (T1) has been interpreted as a transgressive black shale with a maximum flooding zone (mfz) placed at the base of the Zechstein Limestone (Ca1) directly overlying the Kupferschiefer (Paul, 2006). Alternatively, it has been viewed as a condensed section developed on the transgressive Zechstein conglomerate, with the mfz placed within the upper T1 (Strohmenger et al., 1996) (Fig. 1b). Euxinic bottom waters at basin scale were established immediately after flooding of the Permian Basins and are indicated by strong pyritisation and co-precipitation of redox-sensitive trace elements (RSTE) (Wedepohl, 1971; Sweeney et al., 1987; Vaughan et al., 1989) as well as by *Chlorobiaceae*-derived biomarkers (Schwark & Püttmann, 1990; Grice et al., 1997, Pancost et al., 2002). Oxygen-depleted bottom waters may have resulted from the aerobic breakdown of organic matter (OM) due to enhanced primary productivity in nutrient-rich waters and/or from formation of a stable pycnocline prohibiting efficient mixing of the water column in the hydrogeographically restricted Kupferschiefer Sea (Wedepohl, 1971; Vaughan et al., 1989; Paul, 2006).

In this study we investigated sediment sections from the Thuringian Basin as well as from the adjacent Werra-Fulda Basin, representing the southern part of the Kupferschiefer Sea (Fig. 1a). The Thuringian Basin was situated in proximity to the shoreline of the Bohemian Massif, thus comprising contrasting depositional environments, including basinal, marginal (lagoon) and swell settings (Figs. 2, S1 in the supplementary information (SI)). To the west and the southwest

the Thuringian Basin was separated from the Hessian Basin and Werra-Fulda Basin by submarine shoals, where no bituminous strata were deposited. To the north, the Thuringian Basin opened towards the North German Basin, which represented the central part of the Southern Permian Basin, and for which water depths of >300 m have been assumed (Ziegler, 1990; Taylor, 1998; Paul 2006). In contrast, a shallow marine lagoon environment existed in the eastern Thuringian Basin. This lagoon consisted of several depressions surrounded by reef systems that may have impacted on the local hydrogeography and affected water exchange with the central part of the Thuringian Basin (Fig. 2). Eastward of the lagoon, bituminous sediments grade into non-bituminous shallow marine deposits, and further to the east into coastal and fluvial clastics, marking the position of the paleo-coastline. Maximum water depth in the central part of the Thuringian Basin has been estimated to have approached ~200 m, whereas a water depth of ~50 m has been assumed for the eastern lagoon (Paul & Huckriede, 2004). The paleogeographic reconstruction presented here is based on the synthesis of numerous well data (see Fig. S3 in SI). In basin settings the Kupferschiefer formation is represented by a bituminous and laminated clay-/marlstone less than <0.5 m thick, although Kupferschiefer profiles from the Werra-Fulda Basin can reach 1.2 m. In marginal settings the early Kupferschiefer formation is represented by a bioturbated limestone, the so-called Mutterflöz Limestone or Border Dolomite (T1Ca), whereas non-bituminous marls were coevally deposited in swell settings. Further information on the profiles investigated is given in the SI (Figs. S4, S5 in SI).

3. Material and methods

3.1. Sampling and sample preparation

Kupferschiefer (and coeval) sediments analyzed here originate from drill cores provided by the Geological Survey of Thuringia. Specimens from the Ilfeld location have been obtained from sampling a Kupferschiefer profile in the Ilfeld Mine. Samples were crushed and powdered using a disc mill in order to obtain homogenous and representative sample material for bulk geochemical analysis. Powdered samples were dried in an oven at 40°C for 48 hours prior to geochemical analysis.

3.2. TOC and TIC abundance

Total carbon (TC) content was directly measured on powdered sample material using a Vario CNS Elemental Analyzer EL III (Elementar®). Total organic carbon (TOC) content was determined on decalcified samples. Decalcification was achieved by treating samples with HCl (10% and 25%) to remove calcium carbonate and dolomite. Subsequently, the samples were washed and neutralized with deionised water and dried in an oven at 40°C for 48 h. Values determined on decalcified samples were corrected for their carbonate loss to yield original TOC concentrations. The total inorganic carbon (TIC) was calculated by subtracting corrected TOC from TC. Reproducibility and accuracy were checked by running replicate analyses of an in-house standard (sulfanilic acid) and duplicate analysis of samples, and was better than 0.1% (2 S.D., n = 34). The carbonate content was calculated by multiplying the TIC by 8.33 (stoichiometry of $CaCO_3$).

3.3. Elemental concentrations

Major and minor element concentrations were determined using a Perkin Elmer Sciex ELAN 6000 ICP/MS. For each analysis, 0.25 g of each sample was digested with a mixture of hydrofluoric, nitric and perchloric acids and reconstituted in hydrochloric and nitric acids. The analytical accuracy and precision were estimated by measuring sample duplicates, certified reference materials and in-lab standards and was better than 10% for Al, Mo and U. Trace-element data are expressed as "enrichment factors" (EF), where $X_{EF} = [(X/Al)_{sample}/(X/Al)_{PAAS}]$, where PAAS is post-Archean average shale (Taylor & McLennan, 1985), and X and Al are weight concentrations of the element X and Al, respectively.

3.4. Molybdenum isotope analysis

Sample powder aliquots were weighed into Teflon digestion vessels, and an exact mass of a ^{100}Mo- and ^{97}Mo-enriched double-spike solution was added to obtain a total Mo spike/sample ratio of ~0.6. Samples were then digested on a hotplate for 60 hours in a 3:1 mixture of concentrated nitric and hydrochloric acids. Mo was purified using the modified anion

exchange method detailed in Dickson et al. (2016), and subsequently analyzed using a Nu-Plasma Multi-Collector ICP-MS. Isotope ratios were calculated offline and are expressed as $\delta^{98/95}$Mo relative to NIST 3134 (Goldberg et al., 2013; Nägler et al., 2014). Separate digestions of the USGS Devonian Shale standard (SDO-1) yielded a composition of 0.79±0.08‰ (2 S.D., n = 28), which is within uncertainty of the value of 0.80‰ estimated by Goldberg et al. (2013).

3.5. Molecular geochemistry

Bitumen extracts were obtained from sample aliquots using an Accelerated Solvent Extraction (ASE, Dionex) system, using a mixture of dichloromethane and methanol (DCM/MeOH; 93:7, v/v) as extraction solvent. Bitumen extracts were separated into aliphatic, aromatic and NSO fractions by silica gel-column chromatography (8 ml SPE column, 2.8 g Silica 60 mesh, 25 – 40µm) using solvents with increasing polarity. Aliphatic hydrocarbons were eluted with *n*-hexane, aromatic hydrocarbons were eluted using a mixture of *n*-hexane and DCM (3:2, v/v) and NSO compounds were eluted with DCM:MeOH (1:1, v/v). For elemental sulfur removal, activated copper turnings were added to the aliphatic hydrocarbon fraction. GC–MS measurements were performed on an Agilent 5975B MSD interfaced to an Agilent 7890A gas chromatograph (GC) equipped with a DB-1MS capillary column (Agilent DB1-HT; 60 m length, 0.25 mm inner diameter, 25µm film thickness). The temperature program used was: 70°C (5 min isothermal) to 140°C at 10°C/min, then to 325°C at 2°C/min (held for 10 min). The quadrupole mass spectrometer was operating in scan mode in the m/z 50 to 750 range. Compounds of interest were identified via characteristic mass spectra and were integrated manually using the GC/MSD ChemStation Software (Agilent Technologies). For semi-quantitative analysis aromatic fractions were spiked with a known amount of per-deuterated pyrene as internal standard.

4. Results

In order to identify evolutionary trends throughout Kupferschiefer profiles of different thickness, data have been plotted versus % of Kupferschiefer thickness for each section. The organic matter (OM) content is expressed as total organic carbon on a carbonate-free basis

(TOC_{cf}) to correct for highly variable carbonate concentrations between the profiles investigated. Stratigraphic trends of geochemical data and proxies are shown in Figs. 3, 4. Average values and data ranges for the different Kupferschiefer sub-units (T1-I, T1-II, T1-III) are given in Table 1.

4.1. Basinal setting

The TOC_{cf} content at basin settings is variable but follows a similar upwards-decreasing trend in each Kupferschiefer profile (Fig. 3). Highest TOC_{cf} concentrations in the range from 3.1–23.8 wt.% (14.1 wt.% on average) occurred in the T1-I sub-unit. In the T1-II sub-unit absolute TOC_{cf} values varied from 3.0–19.8 wt.% (8.6 wt.% on average) and from 1.6–10.5 wt.% (3.9 wt.% on average) in samples from the T1-III sub-unit. Low TOC_{cf} values <2 wt.% (0.7 wt.% on average) were measured for samples from the Ca1 interval (Fig. 3; Tab. 1).

The stratigraphic trends in Mo_{EF} and U_{EF} were similar throughout the profiles investigated and mimicked the upwards-decreasing TOC_{cf} trend (Fig. 3). Mo_{EF} in samples from T1-I fell in the range from 199–1460 (641 on average), U_{EF} ranged from 24–193 (82 on average). Samples from the T1-II sub-unit contained Mo_{EF} between 48 and 1056 (368 on average) and U_{EF} between 11 and 125 (37 on average). Mo_{EF} between 34 and 390 (135 on average) and U_{EF} between 8 and 38 (18 on average) were determined for samples from the T1-III sub-unit. Mo_{EF} and U_{EF} in samples from the Ca1 were always low (Mo_{EF} <76, 19 on average; and U_{EF} <17, 10 on average) (Fig. 3; Tab. 1). Throughout the T1 facies average Mo_{EF}/U_{EF} ratios ranged from ~8 and ~10. The average Mo_{EF}/U_{EF} ratio for Ca1 deposits was ~2. Average Mo/TOC ratios of 28–32 occurred throughout the T1 facies and ratios of ~18 are found in samples from the basal Ca1 (Fig. 7; Tab. 1).

Molybdenum isotope compositions for basinal successions have been measured for samples from Ilfeld and KalButtlar, where absolute $\delta^{98/95}Mo_{SED}$ values and trends were similar in both profiles. In the T1-I sub-unit $\delta^{98/95}Mo_{SED}$ increased from 0.43‰ to 1.73‰. Afterwards, values stayed consistently high throughout the lower part of the T1-II (1.48–1.76‰), before declining throughout the upper T1-II and the T1-III sub-units to between 0.03–0.30‰ (Fig. 3; Tab. 1).

Biomarker data have been generated for samples from the Ilfeld section. Samples from the T1 facies exhibited an excellent preservation of C_{35} hopanes (expressed as $(C_{35}/\sum_{31\text{-}35})$ x

100), with relative abundances of ~5–7%. For the Ca1 samples the relative abundance of C_{35} hopanes was <5%. DBT/Phen ratios of 0.4–0.6 occurred in samples from the T1-I and T1-II sub-units. T1-III and Ca1 samples had ratios of ~0.1 (Fig. 4; Tab. 1). *Chlorobiaceae*-derived lipids, such as isorenieratane (see introduction), were absent in the samples investigated. Temperature-sensitive biomarker investigations for core KalButtlar were prohibited by the high thermal maturity of the sedimentary OM.

4.2. Marginal settings

Samples from the Mutterflöz (T1Ca) revealed low TOC_{cf} values that ranged from 0.8–3.4 wt.%. Samples from the overlying T1 facies (*sensu stricto*) contained highly variable TOC_{cf} values varying from 0.4–25 wt.%. Highest TOC_{cf} contents that ranged from 17.6–25 wt.% and from 4.3–16.7 wt.% occurred in samples from cores JE106/62 and WisBar, respectively. High TOC_{cf} values in the range 1.4–17.4 wt.% were also measured in samples from cores JE110/62 and JE102/62. Samples from core R14/60 showed moderate TOC_{cf} values that fall in the range 0.4–6 wt.% (Fig. 3; Tab. 1).

Mo_{EF} and U_{EF} of 12–100 and 12–38, respectively, have been determined in samples from core WisBar. Enrichments were also calculated for samples from core R14/60, where Mo_{EF} and U_{EF} ranged from 1–81 and from 6–25, respectively. Mo_{EF} and U_{EF} were higher in core JE106/62, with values ranging from 161–437 and from 35–51, respectively, and in cores JE102/62 and JE110/62 Mo_{EF} and U_{EF}, where they ranged from 12–313 and from 12–98, respectively (Fig. 3; Tab. 1). The average Mo_{EF}/U_{EF} ratio for all marginal sites was ~4. Average Mo/TOC ratios ranged from 11–41 (Fig. 7; Tab. 1).

Molybdenum isotope compositions were measured for samples from cores JE106/62 and WisBar. $\delta^{98/95}Mo_{SED}$ in both cores were quasi-uniform and ranged from 0.70–1.30‰ (Fig. 3; Tab. 1).

Biomarker data have been generated for T1-samples (*sensu stricto*) from cores WisBar and JE106/62. Due to the low OM content Mutterflöz-samples were not suitable for molecular geochemical analysis. The highest relative abundances of C_{35} hopanes were present in samples from JE106/62, where values ranged from 7.7–8.7%. In core WisBar the proportions of C_{35} hopanes fell in the range 5–6%, and declined from the uppermost T1 upwards to a minimum of

1.8% in the sample from Ca1. DBT/Phen ratios were low and uniform (0.1–0.2) in samples from core WisBar, but were more variable in samples from core JE106/62 (0.2–0.5) (Fig. 4; Tab. 1). Isorenieratane has been identified in samples from cores JE106/62 and WisBar at concentrations at 1.1–3.9 µg/gTOC and 0.4–4.2 µg/gTOC, respectively.

4.3. Swell setting

Profiles attributed to a swell setting showed overall low TOC_{cf} contents, ranging from 0.1–1.1 wt.% (0.3 wt.% on average). Mo_{EF} and U_{EF} were low and uniform and ranged from 0.3–90 (10 on average) and 6–29 (12 on average), respectively. Corresponding Mo_{EF}/U_{EF} ratios were below <1 (on average 0.6). The average Mo/TOC ratio was ~20 (Tab. 1). Molecular geochemical investigations were prohibited by the overall low OM contents.

5. Discussion

5.1. Redox conditions in the SE Kupferschiefer Sea

Contrasting Kupferschiefer depositional environments, comprising basinal, marginal and swell settings, can be distinguished from the patterns of Mo, U and OM enrichments. Spatial changes in these parameters can be associated with differences in the redox conditions, controlled in turn by paleogeographic features of the Thuringian Basin.

5.1.1. Basinal setting

The high Mo_{EF} and Mo_{EF}/U_{EF} observed for parallel-bedded/laminated sediments from basinal sites (Figs. 5, 6a) can be explained by the accelerated removal of Mo from the seawater in the presence of aqueous H_2S (Helz et al., 1996, 2011; Algeo & Tribovillard, 2009). The absence of oxygen in bottom waters favored an efficient burial of OM expressed by the high associated TOC_{cf} values (Fig. 5). Euxinic conditions could be inferred also from the biomarker data generated for the Ilfeld section. The excellent preservation of C_{35} hopanes (>5%) supports H_2S-rich bottom waters, promoting the preservation of the homohopane side chain (Sinninghe

339 Damsté et al., 1995). Moreover, high DBT/Phen ratios of ~0.4 corroborated H_2S-rich bottom
340 waters, which in combination with a limited availability of reactive iron, promoted the
341 incorporation of sulfur into organic matter (Hughes et al., 1995). Geochemical data were in
342 accordance with parallel sediment bedding/lamination of the Kupferschiefer deposits indicating
343 bottom waters that were always hostile for benthic organisms (in- and epi-fauna) throughout T1
344 times. Whether euxinic conditions extended into the photic zone cannot be constrained, as
345 diagnostic lipids, like isorenieratane, were not detected in basinal samples. The absence of
346 *Chlorobiaceae*-derived lipids could potentially be explained by euxinic bottom waters limited to
347 the aphotic zone, as water depths of >200 m estimated for the central Thuringian Basin exceed
348 the penetration depth of sunlight (Paul & Huckriede, 2004). However, the absence of
349 *Chlorobiaceae*-derived lipids is insufficient to rule out PZE due to possible diagenetic loss of
350 isorenieratane via thermal breakdown (see Tab. S1 in the SI). Aryl isoprenoids, diagenetic
351 breakdown-products of isorenieratane (see review by Sinninghe Damsté et al., 2001), have been
352 identified in samples from the Ilfeld section, but concentrations were low and the distribution
353 pattern was dominated by short chain aryl isoprenoids ($<C_{18}$) (Fig. S6 in the SI), pointing to only
354 episodic PZE (Schwark & Frimmel, 2004). The occurrence of aryl isoprenoids, however, is no
355 unambiguous evidence for PZE as these compounds can have additional sources other than
356 isorenieratane (e.g. Grice et al., 1996; Koopmans et al., 1996).
357
358 **5.1.2. Marginal settings**
359
360 Deposits in the eastern Thuringian Basin record the presence of a marginal lagoon
361 environment (Paul & Huckriede, 2004). Variable TOC_{cf} and RSTE abundances in combination
362 with location specific trends throughout the T1 facies highlight the role of local
363 paleoceanographic conditions in controlling the redox regime (Fig. 5). On the one hand, profiles
364 JE102/62 and JE110/62, situated in proximity to the open Thuringian Basin, showed high TOC_{cf}
365 values (~8.3 wt.%) and similar U_{EF} and Mo_{EF} to those seen at basin settings. In contrast, the low
366 TOC_{cf} (~2.5 wt.%), U_{EF} (~11) and Mo_{EF} (~9) values in samples from core RU14/60 reflected
367 preferentially suboxic/anoxic conditions, with a chemocline situated within the sediment or
368 probably close to the sediment-water interface.

Cores JE106/62 and WisBar derived from hydrogeographically restricted lagoon environments (Figs. 2, 5), with water depths of ~50 m (Paul & Huckriede, 2004). The high TOC_{cf} enrichments in both cores indicated excellent conditions for OM preservation. Moreover, the presence of isorenieratane suggested the occurrence of PZE, which is in agreement with the excellent preservation of C_{35} hopanes (Fig. 4). This inference is also supported by the observation that long-chain aryl isoprenoids ($>C_{18}$) occurred in significant amounts (Fig. S6 in the SI), pointing to a stable chemocline situated within the water column (Schwark & Frimmel, 2004), and by the lack of sedimentological evidence for benthic activity throughout T1 times. Differences between the two lagoonal sites were apparent, however. High DBT/Phen ratios of ~0.4 in samples from core JE106/62 pointed to the limited availability of reactive iron in the Jena Lagoon, promoting the enhanced incorporation of sulfur into OM (Hughes et al., 1995). This situation was not apparent in samples from core WisBar, where low DBT/Phen ratios of ~0.2 could be explained by the enhanced availability of iron, perhaps supplied via riverine delivery. According to the paleogeographic reconstruction, core WisBar was located close to an estuary in the Gera Lagoon, which may have enhanced freshwater fluxes (and suspended sediment loads) to this location (Figs. 2, 5). The existence of river systems supplying clastic sediment from the Variscian Orogen to the southern part of the Southern Permian Basin has been supported by sedimentological observations (Ziegler, 1990; Kiersnowski et al., 1995).

Further differences between the two lagoonal sites are indicated by the patterns of Mo_{EF}/U_{EF} co-variation. High U_{EF} and Mo_{EF}, and high Mo_{EF}/U_{EF} ratios from core JE106/62 were consistent with the presence of basin euxinia. However, samples from core WisBar showed lower values for these parameters, which could be attributed to less reducing conditions. This situation, however, would be inconsistent with the biomarker data for stable photic zone euxinia (discussed above) and thus, other mechanisms than the redox regime must have impacted on the RSTE accumulation in core WisBar (see discussion in 5.3.).

5.1.3. Swell setting

Bioturbated marlstones at the Langensalza Swell could be attributed to a swell facies type (Fig. 2). The low U_{EF} (<15), Mo_{EF} (<12) and Mo_{EF}/U_{EF} (Tab. 1) along this paleo-elevation indicate sediments deposited in oxic/suboxic conditions (Algeo & Tribovillard, 2009;

Tribovillard et al., 2012). These conditions were not favorable for OM preservation as indicated by low TOC_{cf} values (<1 wt.%). Geochemical data were in agreement with sedimentological observations and attested that the chemocline was situated within the sediment (Fig. S4).

5.2. Stratigraphic trends and controls on redox conditions

The trace metal distributions and biomarker data at basinal sites suggested that euxinic conditions were established immediately after formation of the Kupferschiefer Sea and persisted throughout T1-I and early T1-II times (Figs. 6a, 7). An efficient burial of OM under euxinic conditions was indicated by high TOC_{cf} contents, high abundances of C_{35} hopanes (>5%) and high DBT/Phen ratios (>0.4) (Figs. 3, 4). The decline of these parameters throughout late T1-II and T1-III times could be attributed to a decline in aqueous H_2S concentrations before preferentially suboxic conditions became established in the lowermost Ca1 interval (Fig. 7). This pattern was in agreement with previous interpretations of the redox evolution of the Kupferschiefer Sea (e.g. Vaughan et al., 1989; Grice et al., 1996, 1997; Sun & Püttmann, 1997). The common response patterns at basin sites indicated a similarity in the basin-wide processes controlling redox.

At marginal sites the early phase of the T1-I transgression was represented by the Mutterflöz limestone (T1Ca), underlying the bituminous T1 facies (*sensu stricto*) (Paul et al., 1982; 2006; Vaughan et al., 1989). The low Mo_{EF}/U_{EF} ratios and low TOC_{cf} values characteristic for the bioturbated Mutterflöz implied the presence of oxygen-replete bottom waters (Figs. 3, 7). However, more reducing conditions during deposition of the Mutterflöz could be inferred from the site JE102/62 data, where Mo_{EF}/U_{EF} of ~5 in association with TOC_{cf} values up to ~5 wt.% have been observed. The sharp transition between the bioturbated Mutterflöz and the overlying bituminous T1 facies (*sensu stricto*), deposited under anoxic to euxinic conditions, points to a rapid depletion of oxygen at marginal settings after a critical water depth was reached. The return to oxic-suboxic conditions in the lowermost Ca1 unit occurred rapidly at sites JE106/62 and WisBar, whereas a more gradual return to oxic-suboxic conditions has been observed at locations more proximal to the open Thuringian Basin (e.g. JE102/62; Figs. 2, 5). The delayed onset of euxinia at marginal settings as well as overall oxic/suboxic conditions at swell settings

highlighted the role of sea level evolution and paleogeography on temporal changes in redox conditions (see section 6).

Factors contributing to the breakdown of bottom water euxinia in the Kupferschiefer Sea have been debated (e.g. Paul, 2006). Sea-level evolution might have played an important role by affecting basin-wide water mass circulation patterns, deepwater renewal times, and oxygen availability. Changes in circulation patterns and in hydrologic conditions might also have resulted from the formation of a connection between Kupferschiefer Sea and Paleo-Tethys via the eastern part of the Southern Permian Basin, which may have occurred during the interval of highest sea-level in the lower Ca1 (Paul, 2006) or the upper T1 interval (Strohmenger et al., 1996). Additionally, a change in climate conditions could have impacted on redox conditions. Deepwater ventilation rates could have been altered by the impact of precipitation and evaporation on surface water stratification. However, changes in stratification could also have affected the recycling of sub-surface nutrients to surface waters (Brongersma-Sanders, 1966, 1971). A consequent decline in the primary productivity throughout T1 times, evident from the evolution of $\delta^{13}C$ values of biomarkers (Grice et al., 1997), may have allowed oxygen concentrations in bottom waters to subtly increase. The role of primary productivity in controlling the redox regime could be indicated by the coupling of OM and RSTE accumulation (TOC_{cf} versus Mo_{EF}: R^2 = ~0.83), suggesting that the extent of sulfate reduction and H_2S production was bound to the availability of degradable OM (Fig. 6b). However, the apparent coupling of OM concentrations with RSTE concentrations could also indicate that OM burial rates were simply controlled by bottom water redox, under a constant flux of exported OM. It is likely that interaction between these mechanisms may have ultimately caused the breakdown in bottom water anoxia/euxinia in the Kupferschiefer Sea.

5.3. Hydrogeographic restriction of the Kupferschiefer Sea

5.3.1. Basinal setting

Despite evidence for euxinia in the southern Kupferschiefer Sea (at least during T1-I and T1-II times), Mo/TOC relationships suggest that aqueous Mo concentrations did not become significantly depleted (Figs. 6b, 7). The lack of significant Mo-depletion can be explained by the fact that the Kupferschiefer Sea had a connection with the Arctic Ocean via the Norwegian-

Greenland Seaway, and potentially a temporary connection with Paleo-Tethys during a sea-level highstand in the upper T1 (Strohmenger et al., 1996) or in the lower Ca1 (Paul, 2006) interval (Fig. 1). These connections would have facilitated a continuous inflow of open marine Mo-replete waters, which would counteract a drawdown of aqueous Mo in the Kupferschiefer Sea under euxinic conditions. Mo_{EF}/U_{EF} ratios for the basin sites (Fig. 6a) support this model by plotting along the trend commonly documented for open marine environments with relatively rapid deepwater renewal (Algeo & Tribovillard, 2009; Tribovillard et al., 2012).

5.3.2. Marginal settings

Unlike for the basinal locations, hydrogeographic restriction during T1 times could be inferred for marginal/lagoonal sites JE106/62 and WisBar on the basis of very low Mo/TOC ratios of ~7–12 for the samples deposited under euxinic conditions at these sites (Fig. 6b). A depletion of aqueous Mo could have been promoted by the restricted setting of both locations that were situated between reef belts, prohibiting an efficient water exchange between the lagoon and the open Thuringian Basin (Figs. 2, 5). In contrast to the Mo/TOC relationships, Mo_{EF}/U_{EF} ratios from JE106/62 and WisBar plot along an open marine trend, which would be inconsistent with extensive RSTE drawdown (Fig. 6a). One possibility for explaining the difference in the two indices is the mixing of RSTE-depleted freshwater into the lagoonal waters (Palmer & Edmond, 1993; Archer & Vance, 2008). As mentioned above, there is strong paleogeographic evidence (e.g. deltaic sediments; also see Ziegler, 1990; Kiersnowski et al., 1995) that the lagoon environment in the eastern Thuringian Basin was influenced by fluvial runoff that may have impacted on the local water chemistry. Limited water exchange with the open Thuringian Basin due to hydogeographic barriers (reef belts) could have enhanced the impact of freshwater discharge on the local seawater chemistry. Under such specific conditions, prolonged euxinia would be unlikely to result in a significant enrichment of Mo, U, or other RSTE in the sediments.

5.4. Molybdenum isotope signature

5.4.1. Basinal setting

The Ilfeld and KalButtlar profiles exhibited extremely similar $\delta^{98/95}Mo_{SED}$ trends (Fig. 3). Samples from the T1-II and T1-III sub-units, as well as from the Ca1 interval, showed a strong correlation of $\delta^{98/95}Mo_{SED}$ with Mo_{EF} ($R^2 = 0.78$), indicating that variations in the abundance and isotopic composition of sedimentary Mo were both controlled by the changing redox environment (aqueous H_2S concentrations), and thus the balance between Mo-sulfide and Mo-oxide deposition (Poulson et al., 2006).

Samples from the T1-I sub-unit at both sites deviated from this redox trend by having high Mo_{EF} with only moderate $\delta^{98/95}Mo_{SED}$ (0.43–1.24‰) (Fig. 8). Mixing of Mo-oxide and sulfide phases in anoxic water resulting in an isotopic difference between aqueous Mo and sedimentary Mo (ΔMo) of >0.70‰ could potentially explain the relatively lowered $\delta^{98/95}Mo_{SED}$ values (Neubert et al., 2008; Nägler et al., 2011). However, they would be difficult to reconcile with high Mo_{EF}, high DBT/Phen ratios and high abundances of C_{35} hopanes, which attested to the presence of H_2S-rich waters. Alternatively, the difference between the T1-I $\delta^{98/95}Mo$ compositions and the inferred redox trend (Fig. 8) could be explained by the admixture of Mo with a lower $\delta^{98/95}Mo$ signature into the basin waters. Open ocean seawater entering the Kupferschiefer Sea may have had a $\delta^{98/95}Mo_{SW} \approx 2.30$‰ (Proemse et al., 2013). Flooding was associated with the intensive reworking and leaching of pre-existing strata, in particular Rotliegend clastics (Wedepohl, 1971; Vaughan et al., 1989; Gast et al., 2010), which could have released buried lithogenic Mo (Mo_{LITH}) with an isotopic composition comparable to crystalline rocks ($Mo_{LITH} \approx$ -0.27‰, Barling et al., 2001; Siebert et al., 2003). The impact of Mo_{LITH} admixture is interpreted to have been most pronounced during T1-I times, and was alleviated by the continuous inflow of open ocean seawater along with the progressive burial of Rotliegend clastics during T1-II and T1-III (Fig. 8).

The positive relationship between Mo concentrations and $\delta^{98/95}Mo$ suggested that local changes in redox controlled the speciation, and hence isotopic composition, of sedimentary Mo. A negative correlation between these two parameters, which would support a hydrographic (basin drawdown) control on the sedimentary $\delta^{98/95}Mo$ (Dickson et al., 2016), was not apparent. It could therefore be inferred that the $\delta^{98/95}Mo$ of ~1.70‰ in the T1-II interval at core KalButtlar and Ilfeld recorded deposition of Mo-sulfides with ΔMo of ~0.70‰ from Kupferschiefer Sea seawater (cf. Poulson et al., 2006; Poulson-Brucker et al., 2009; 2012; Dickson et al., 2014, 2016). The minimum isotopic composition of aqueous Mo in the Kupferschiefer Sea ($\delta^{98/95}Mo_{KS-}$

523 $_{SW}$) during T1-II times could therefore be estimated at ~2.40‰, which is close to the ~2.30‰
524 estimated for the Late Permian open ocean (Proemse et al., 2013). This similarity suggested a
525 strong chemical connection between the Kupferschiefer Sea and the Permian open ocean. The
526 ongoing decrease in $\delta^{98/95}Mo_{SED}$ values throughout the upper T1-II and the T1-III sub-units
527 might either have been due to a secular shift in the $\delta^{98/95}$Mo of Permian seawater, or due to a
528 progressive increase in the mixture of oxide-bound Mo to the Kupferschiefer sediments under
529 better ventilated bottom waters. The latter suggestion was consistent with the U_{EF}-Mo_{EF} patterns
530 and with biomarker data (Figs. 3, 4).
531
532 **5.4.2. Lagoonal setting**
533
534 The relatively low $\delta^{98/95}Mo_{SED}$ of 0.70–1.30 ‰ at the lagoonal sites compared to the basin
535 sites could be explained by the mixing of Mo-oxides and thiomolybdates in the former settings
536 (Siebert et al., 2006; Poulson-Brucker et al., 2009). This process would, however, contradict
537 sedimentological observations and biomarker data, which attested to H_2S-rich waters extending
538 into the photic zone of the lagoon waters. Assuming that sedimentary Mo instead was dominated
539 by thiomolybdates with an approximate offset from coeval lagoonal waters of ~0.70 ‰ would
540 imply that the Mo-isotope composition lagoon seawater ($\delta^{98/95}Mo_{LSW}$) was ~1.8 ‰, which is
541 substantially lower than that of the basinal waters (see above). This difference in seawater
542 chemical composition could be explained by the admixture of Mo-replete fluvial-derived
543 freshwater into the lagoonal waters. Mass balance calculations indicated that a local $\delta^{98/95}Mo_{LSW}$
544 value of ~1.80‰ can be achieved by a freshwater:seawater mixing ratio of 9:1, when assuming a
545 seawater Mo concentration of ~105 nmol/l with a $\delta^{98/95}Mo_{KS\text{-}SW}$ value of ~2.40‰ and a
546 freshwater Mo concentration of ~6 nmol/l with an isotopic composition of 0.44‰ (average
547 modern river values (Archer & Vance, 2008) (Fig. 10). This is, however, only an approximate
548 estimate as the concentration and isotopic composition of Mo in present-day river waters can be
549 highly variable (Archer & Vance, 2008; Wang et al., 2015). Moreover, aqueous Mo
550 concentrations in the open Thuringian Basin could have been declined to values <105 nmol/l
551 during T1-I and T1-II times, due to high Mo burial rates. A near-quantitative drawdown of the
552 aqueous Mo at site WisBar was indicated by low Mo/TOC ratios ~7 (Fig. 7), which could have
553 driven the ΔMo closer to a calculated tetrathiomolybdate difference from seawater of ~0.5‰

(Nägler et al., 2011), resulting in its slightly higher $\delta^{98/95}Mo_{SED}$ composition compared with site JE106/62 (Fig. 10).

6. Depositional model – a synthesis

A depositional model for the southern Kupferschiefer of the Thuringian Basin could be constructed from the new organic and inorganic data, which explained the observed temporal and spatial variations in redox and hydrologic conditions. At basin settings, euxinic conditions with aqueous H_2S concentrations </= 11µmol/l were established immediately after formation of the Kupferschiefer Sea, as indicated by high accumulation rates of RSTE, high DBT/Phen ratios and the high abundance of C_{35} hopanes. During T1-I times, high rates of Mo accumulation in basinal sediments were accompanied by relatively low $\delta^{98/95}Mo_{SED}$ values, reflecting the admixture of isotopically light lithogenic Mo released from pre-existing clastic deposits during inundation of the European Permian Basins (Fig. 11a). Mo/TOC and Mo_{EF}/U_{EF} relationships argued against widespread RSTE drawdown in the southern Kupferschiefer Sea, implying that $MoO_xS_{4-x}^{2-}$ species were fractionated from aqueous MoO_4^{2-} by ~ 0.70 ‰, the difference between the Mo-isotope composition of modern seawater and Mo-sulfides deposited in Mo-replete environments (Poulson-Brucker et al., 2009, 2012; Dickson et al., 2014, 2016). The highest $\delta^{98/95}Mo_{SED}$ value of ~1.70‰ consequently equated to a $\delta^{98/95}Mo_{KS\text{-}SW}$ value of ~2.4‰, which is similar to an existing estimate of Late Permian open ocean seawater (Proemse et al., 2013).

Quantitative drawdown of aqueous Mo in the southern Kupferschiefer Sea was prohibited by multiple factors including: i) high initial aqueous Mo concentrations in the earliest Kupferschiefer Sea due to the admixture of lithogenic Mo liberated during the initial stages of basin flooding and by continuous resupply from the open ocean during ongoing transgression; ii) low aqueous H_2S concentrations <11 µmol/l; and iii) a decline in Mo burial rates during deposition of the upper T1-II and the T1-III sub-units due to a shift towards more oxygenated basin waters (Fig. 11c).

The onset of euxinic conditions at marginal lagoon sites was delayed compared to basinal sites. This delay could be attributed to the paleogeography of the Thuringian basin, which prevented low-oxygen waters from occupying the shallow marginal lagoonal sites during the T1-I interval. Subsequently, the very high abundance of C_{35} hopanes and the occurrence of

585 isorenieratane implied that euxinic conditions prevailed during T1-II and T1-III times, most
586 likely due to basin flooding from the ongoing transgression (Fig. 11c). Corresponding moderate
587 $\delta^{98/95}Mo_{SED}$ values of only ~1‰, which were notably lower than in the basinal successions, could
588 be explained by the admixture of Mo-depleted riverine freshwater with a lower isotopic
589 composition (Archer & Vance, 2008). The fact that freshwater input was able to exert a strong
590 control on $\delta^{98/95}Mo_{SED}$, rather than simply forming a salinity 'cap,' suggests that the lagoonal
591 basins were shallow enough to enable periodic mixing to the basin floor (Fig. 11c).
592 The occurrence of isorenieratane, diagnostic for green sulfur bacteria, at marginal lagoon
593 sites attested to near shore euxinia that extended into the photic zone. At basinal sites evidence
594 for the occurrence of green sulfur bacteria is missing, most likely due to the thermal breakdown
595 of isorenieratane. Alternatively, the absence of *Chlorobiaceae*-derived lipids may indicate that in
596 the Thuringian Basin euxinic conditions were limited to the aphotic zone. This differs from PZE
597 documented for basinal settings in the Lower Rhine Embayment and the Yorkshire Basin
598 (Schwark and Püttmann, 1990; Pancost 1992) of the SPB as well as the Norwegian Danish Basin
599 in the NPB (Pancost et al., 1992).
600
601 **7. Conclusions**
602
603 The combined inorganic and organic geochemical approaches allowed a detailed
604 reconstruction of paleoenvironmental conditions in the Thuringian Basin during deposition of the
605 Kupferschiefer. The new data supported the argument that paleogeographic features of the
606 Thuringian Basin controlled spatial changes in redox conditions, whereas temporal changes in
607 redox were predominantly governed by sea level evolution and organic matter productivity. Mo-
608 isotope and metal enrichments indicated that prolonged euxinia in the semi-enclosed
609 Kupferschiefer Sea did not lead to a near-quantitative depletion of the aqueous Mo reservoir.
610 Trends in U_{EF}, Mo_{EF} and TOC_{cf} patterns followed an evolution typical for open marine,
611 hydrographically unrestricted settings, and were likely governed by the continuous resupply of
612 Mo from the open ocean during ongoing transgression in combination with short deepwater
613 renewal times and a decline in Mo-burial rates during late T1 and Ca1 times. The isotopic
614 composition of sedimentary Mo at basins settings was primary controlled by the prevailing local
615 redox state, with an additional contribution of lithogenic Mo released from leached Rotliegend

clastics during T1-I times. The highest $\delta^{98/95}Mo_{SED}$ values of ~1.70‰ were thus likely to record a -0.70‰ fractionation of Mo-sulfides from aqueous Mo, thereby setting the $\delta^{98/95}Mo_{KS\text{-}SW}$ value of ~2.40‰. This estimate was similar to a value of ~2.30‰ measured from Upper Permian black shales in the Sverdrup Basin (Proemse et al., 2013), and hence supported the notion that it closely approximated upper Late Permian open-ocean seawater. The accumulation of RSTE and the Mo-isotope composition of sediments in marginal lagoonal settings were affected by Mo-depleted freshwater fluxes that had a strong influence on the local seawater chemistry and the isotopic composition of the aqueous Mo reservoir. Redox-controlled biomarker proxies were not affected by seawater chemistry and thus provided hydrologically independent information on the redox and depositional conditions, suggesting the presence of at least episodic PZE. This study further demonstrated that deposition of organic matter and metals in the Kupferschiefer was a phenomenon strongly linked to basin-scale controls, and therefore differed from the Mesozoic OAEs, which experienced global-scale controls (e.g. LIP volcanism) that influenced carbon burial at a wider spatial scale. This difference was reflected in the inferred seawater Mo-isotope composition for the Late Permian, which at 2.30–2.40‰, was significantly higher than the composition inferred for OAE-2 (~1.2‰, Westermann et al., 2014; Dickson et al., 2016), reflecting a better-oxygenated ocean worldwide.

Acknowledgment

We like to thank Dr. Hermann Huckriede (Geological Survey of Thuringia, Germany) for providing the sample material and for information on the geological background. We appreciate the constructive and helpful comments of T.J. Algeo and an anonymous reviewer that helped to improve the manuscript.

REFERENCES CITED

Algeo, T.J., Tribovillard, N., 2009. Environmental analysis of paleoceanographic systems based on molybdenum–uranium covariation. Chemical Geology 268, 211 – 225.

Algeo, T.J., Lyons, T.W., 2006. Mo-total organic carbon covariation in modern anoxic marine environments: implication for analysis of paleoredox and -hydrographic conditions. Paleoceanography 21, PA1016.

Algeo, T.J., Maynard, J.B., 2008. Trace metal covariation as a guide to water-mass conditions in

ancient anoxic marine environments. Geosphere 4, 872 – 887.

Algeo, T.J., Rowe, H., 2012. Paleoceanographic applications of trace-metal concentration data. Chemical Geology 324 – 325, 6 – 18.

Archer, C., Vance, D., 2008. The isotopic signature of the global riverine molybdenum flux and anoxia in the ancient ocean. Nature Geoscience 1, 597 – 600.

Arnold, G. L., Anbar, A.D., Barling, J., Lyons, T.W., 2004. Molybdenum isotope evidence for widespread anoxia in mid-Proterozoic oceans, Science, 304, 87–90.

Barling, J., Anbar, A.D., 2004. Molybdenum isotope fractionation during adsorption by manganese oxides. Earth and Planetary Science Letters 217, 315 – 329.

Barling, J., Arnold, G.L., Anbar, A.D., 2001. Natural mass-dependent variations in the isotopic composition of molybdenum. Earth and Planetar Science Letters 193, 447 – 457.

Brongersma-Sanders, M., 1966. Metals of the Kupferschiefer supplied by normal seawater. Geologische Rundschau 55, 365 – 375.

Brongersma-Sanders, M. 1971. Origin of major cyclicity of evaporites and bituminous rocks: an actualistic model. Marine Geology 11, 123 – 144.

Crusius, J., Calvert, S., Pedersen, T., Sage, D., 1996. Rhenium and molybdenum enrichments in sediments as indicators of oxic, suboxic and sulfidic conditions of deposition. Earth and Planetary Science Letters 145, 65 – 78.

Dickson, A.J. and Cohen, A.S., 2012. A molybdenum isotope record of Eocene Thermal Maximum 2: implications for global ocean redox during the Early Eocene. Paleoceanography 27, PA3230, doi:10.1029/2012PA002346.

Dickson, A.J., Cohen, A.S., Coe, A.L., 2014. Continental margin molybdenum isotope signatures from the early Eocene. Earth and Planetary Science Letters 404, 389 – 395.

Dickson, A.J., Jenkyns, H.C., Porcelli, D., van den Boorn, S., Idez, E., 2016. Basin-scale controls on the molybdenum-isotope composition of seawater during Oceanic Anoxic Event 2 (Late Cretaceous). Geochimica et Cosmochimica Acta 178, 291 – 306.

Emerson, S.R., Huested, S.S., 1991. Ocean anoxia and the concentrations of molybdenum and vanadium in seawater. Marine Chemistry 34, 177 – 196.

Erickson, B.E., Helz, G.R., 2000. Molybdenum (VI) speciation in sulfidic waters: Stability and lability of thiomolybdates. Geochimica et Cosmochimica Acta 64, 1149 – 1158.

Gast, R., Dusar, M., Breitkreuz, C., Gaupp, R., Scheider, J.W., Stemmerik, L., Geluk, M.,

678 Geissler, M., Kiersnowski, H., Glennie, K., Kabel, S., Jones, N., 2010. Rotliegend. In:
679 Doornenbal, J.C., Stevenon, A.G., (Eds.) Petroleum Geological Atlas of the Southern
680 Permian Basin Area. EAGE Publication b.v. (Houten), p. 123 – 148.
681 Grice, K., Schaeffer, P., Schwark, L., Maxwell, J.R., 1996. Molecular indicators of
682 palaeoenvironmental conditions in an immature Permian shale (Kupferschiefer, Lower
683 Rhine Basin, north-west Germany) from free and S-bound lipids. Organic Geochemistry 25,
684 131 – 147.
685 Grice, K., Schaeffer, P., Schwark, L., Maxwell, J.R., 1997. Changes in palaeoenvironmental
686 conditions during deposition of the Permian Kupferschiefer (Lower Rhine Basin, northwest
687 Germany) inferred from molecular and isotopic compositions of biomarker components.
688 Organic Geochemistry 26, 677 – 690.
689 Glennie, G.T., Buller, A.T., 1983. The Permian Weißliegend of NW Europe: the partial
690 deformation of eolian sands caused by the Zechstein transgression. Sedimentary Geology
691 35, 43 – 81.
692 Goldberg, T., Archer, C., Vance, D., Poulton, S.W., 2009. Mo isotope fractionation during
693 adsorption to Fe (oxyhydr)oxides. Geochimica et Cosmochimica Acta 73, 6502 – 6516.
694 Goldberg, T., Gordon, G., Izon, G., Archer, C., Pearce, C.R., McManus, J., Anbar, A.D.,
695 Rehkämper, M., 2013. Resolution of inter-laboratory discrepancies in Mo isotope data: an
696 intercalibration. Journal of Analytical Atomic Spectrometry 28, 724 – 735.
697 Helz, G.R., Miller, C.V., Charnock, J.M., Mosselmans, J.F.W., Pattrick, R.A.D., Gerner, C.D.
698 and Vaughan, D.J., 1996. Mechanism of molybdenum removal from the sea and its
699 concentration in black shales: EXAFS evidence. Geochimica et Cosmochimica Acta 60,
700 3631–3642.
701 Helz, G.R., Bura-Nakić, E., Mikac, N., Ciglenečki, I., 2011. New model for molybdenum
702 behavior in euxinic waters. Chemical Geology 284, 323 – 332.
703 Hughes, W.B., Holba, A.G., Dzou, L.I.P., 1995. The ratio of dibenzothiophene to phenanthrene
704 and pristane to phytane as indicator of depositional environment and lithology of petroleum
705 source rocks. Geochimica et Cosmochimica Acta 59, 3581 – 3598.
706 Kiersnowski, H., Paul, J., Peryt, T.M:, Smith, D.S., 1995. Facies, paleogeography, and
707 sedimentary history of the Southern Permian Basin in Europe. In: Scholle, P.A., Peryt, T.M.,
708 Ulmer-Scholle, D.S., (Eds.) The Permian of northern Pangaea 2, Sedimentary Basins and

Economic resources. Springer, pp. 119 – 136.

Koopmans, M.P., Schouten, S., Kohnen, M.E.L., Sinninghe Damsté, J.S., 1996. Restricted utility of aryl isoprenoids as indicators for photic zone anoxia. Geochimica et Cosmochimica Acta 60, 4873 – 4876.

Nägler, T.F., Neubert, N., Böttcher, M.E., Dellwig, O., Schnetger, B., 2011. Molybdenum isotope fractionation in pelagic euxinia: Evidence from the modern Black and Baltic Seas. Chemical Geology 289, 1 -11.

Nägler T.F., Anabar, A.D., Archer, C., Goldberg, T., Gordon, G.W., Greber, N.D., Siebert, C., Sohrin, Y., Vance, D., 2014. Proposal for an international molybdenum isotope measurement standard and data representation. Geostandards and Geoanalytical Resarch 38, 149 – 151.

Neubert, N., Nägler, T.F., Böttcher, M.E., 2008. Sulfidity controls molybdenum isotope fractionation into euxinic sediments: Evidence from the modern Black Sea. Geology 36, 775 – 778.

Ogg, J.G., Ogg, G.M., Gradstein, F.M., 2016. A concise geological timescale. Elsevier, 240 pp.

Palmer, M.R., Edmond, J.M., 1993. Uranium in river water. Geochimica et Cosmochimica Acta 57, 4947 – 4955.

Pancost, D.R., Crawford, N., Maxwell, J.R., 2002. Molecular evidence for basin-scale photic zone euxinia in the Permian Zechstein Sea. Chemical Geology 188, 217 – 227.

Paul, J., 1982. Zur Rand- und Schwellen-Fazies des Kupferschiefers. Zeitschrift der deutschen geologischen Gesellschaft 133, 571 – 605.

Paul, J., 2006. Der Kupferschiefer: Lithologie, Stratigraphie, Fazies und Metallogenese eines Schwarzschiefers. Zeitschrift der Deutschen Gesellschaft für Geowissenschaften 157, 57 – 76.

Paul, J., Huckriede, H., 2004. Riffe, Gips und Erze: Zechstein zwischen Saalfeld und Neustadt/Orla. Schriftenreihe der Deutschen Geologischen Gesellschaft 35, 75 – 91.

Pearce, C.R., Cohen, A.S., Parkinson, I.J., 2009. Quantitative separation of molybdenum and rhenium from geological materials for isotopic determination by MC-ICP-MS. Geostandards and Geoanalytical Research 33, 219–229.

Peryt, T.M., Geluk, M., Mathiesen, A., Paul, J., Smith, K., 2010. Zechstein. In: Doornenbal, J.C., Stevenon, A.G., (Eds.) Petroleum Geological Atlas of the Southern Permian Basin Area.

740 EAGE Publication b.v. (Houten), p. 123 – 148.
741 Peters, K.E., Walters, C.C., Moldowan, J.M., 2005. The Biomarker Guide: Volume 2,
742 Biomarkers and Isotopes in Petroleum Systems and Earth History. Cambridge University
743 Press, 1132 p.
744 Poulson, R.L., Siebert, C., McManus, J., Berelson, W.M., 2006. Authigenic molybdenum isotope
745 signatures in marine sediments. Geology 34, 617 – 620.
746 Poulson-Brucker R.L., McManus J., Severmann S., Berelson, W.M., 2009. Molybdenum
747 behavior during early diagenesis: insights from Mo isotopes. Geochemistry, Geophysics,
748 Geosystems 10, Q06010. http://dx.doi.org/10.1029/2008GC002180.
749 Poulson-Brucker R.L., McManus J., Poulton S.W., 2012. Molybdenum isotope fractionations
750 observed under anoxic experimental conditions. Geochemical Journal 46, 201 – 209.
751 Proemse, B.C., Grasby, S.E., Wieser, M.E., Mayer, B., Beauchamp, B., 2013. Molybdenum
752 isotopic evidence for oxic marine conditions during the latest Permian extinction. Geology
753 doi: 10.1130/G34466.1
754 Siebert, C., Nägler, T.F., von Blanckenburg, F., Kramers, J.D., 2003. Molybdenum isotope
755 records as a potential new proxy for paleoceanography. Earth and Planetary Science Letters
756 211, 159 – 171.
757 Siebert, C., McManus, J., Bice, A., Poulson, R., Berelson, W.M., 2006. Molybdenum isotope
758 signatures in continental margin marine sediments. Earth and Planetary Science Letters 241,
759 723 – 733
760 Schwark, L., Püttmann, W., 1990. Aromatic composition of the Permian Kupferschiefer in the
761 Lower Rhine Basin, NW Germany. Organic Geochemistry 16, 749 – 761.
762 Schwark, L., Frimmel, A., 2004. Chemostratigraphy of the Posidonia Black Shale, SW-
763 Germany: II. Assessment of extent and persistence of photic-zone anoxia using aryl
764 isoprenoid distributions. Chemical Geology 206, 231 – 248.
765 Sinninghe Damsté, J.S., Schouten, S., 2006. Biological markers for anoxia in the photic zone of
766 the water column. In: Volkman (Ed.), Marine Organic Matter. Springer Verlag, Heidelberg,
767 p. 127 – 163.
768 Sinninghe Damsté, J.S., Schouten, S., van Duin, A.C.T., 2001. Isorenieratene derivatives in
769 sediments: Possible controls on their distribution. Geochimica et Cosmochimica Acta 65,
770 1557 – 1571.

771 Sinninghe Damsté, J.S., Van Duin, A.C.T., Hollander, D., Kohnen, M.E.L., De Leeuw, J.W.,
772 1995. Early diagenesis of bacteriohopanepolyol derivatives: Formation of fossil
773 homohopanoids. Geochimica et Cosmochimica Acta 59, 5141 – 5155.
774 Stollhofen, H., Bachmann, G.H., Barnasch, J., Bayer, U., Beutler, G., Franz, M., Kästner, M.,
775 Legler, B., Mutterlose, J., Radies, D., 2008. Upper Rotliegend to Early Cretaceous basin
776 development, In: Littke, R., Bayer, U., Gajewski, D., Nelskamp, S. (Eds.), Dynamics of
777 complex intracontinental basins. The Central European Basin System: Berlin, Springer-
778 Verlag, p. 191 – 210.
779 Strohmenger, C., Voigt, E., Zimdars, J., 1996. Sequence stratigraphy and cyclic development of
780 Basal Zechstein carbonate-evaporite deposits with emphasis on Zechstein 2 off-platform
781 carbonates (Upper Permian, Northeast Germany). Sedimentary Geology 102, 33 – 54.
782 Summons, R.E., Powell, T.G., 1986. Chlorobiaceae in Palaeozoic seas revealed by biological
783 markers, isotopes and geology. Nature 319, 763 – 765.
784 Sun, Y., Püttmann, W., 1997. Metal accumulation during and after deposition of the
785 Kupferschiefer from the Sangerhausen Basin, Germany. Applied Geochemistry 12, 577 –
786 592.
787 Sweeney, M., Turner, P., Vaughan, D. J., 1987. The Marl Slate: A model for the precipitation of
788 calcite, dolomite and sulfides in a newly-formed anoxic sea. Sedimentology 34, 31 – 48.
789 Szurlies, M., 2013. Late Permian (Zechstein) magnetostratigraphy in Western and Central
790 Europe. In: Gasiewicz, A., Slowakiewicz, M., 2013 (Eds.). Palaeozoic Climate Cycles: Their
791 Evolutionary and Sedimentological Impact. Geological Society Special Publications 376, pp.
792 73 – 86.
793 Taylor, J.C.M., 1998. Upper Permian-Zechstein. In: Glennie, K.W. (Ed.), Introduction to the
794 Permian Geology of the North Sea. Blackwell Scientific Publications, Oxford, pp. 153 –
795 189.
796 Taylor, S.R., McLennan, S.M., 1985. The continental crust: its composition and evolution.
797 Blackwell, Oxford. 312 p.
798 Tribovillard, N., Algeo, T.J., Lyons, T., Riboulleau, A., 2006. Trace metals as paleoredox and
799 paleoproductivity proxies: An update. Chemical Geology 232, 12 – 32.
800 Tribovillard, N., Algeo, T.J., Baudin, F., Riboulleau, A., 2012. Analysis of marine environmental
801 conditions based on molybdenum–uranium covariation - Applications to Mesozoic

paleoceanography. Chemical Geology 324 – 325, 46 – 58.

Vaughan, D.J., Sweeney, M., Friedrich, G., Diedel, R., Haranczyk, C., 1989. The Kupferschiefer: an overview with an appraisal of the different types of mineralization. Economic Geology 84, 1003 – 1027.

Wang, Z., Ma, J., Li, J., Wei, G., Chen, X., Deng, W., Xie, L., Lu, W., Zou, L., 2015. Chemical weathering controls on variations in the molybdenum isotopic composition of river water: Evidence from large rivers in China. Chemical Geology 410, 201 – 212.

Wedepohl, K.H., 1964. Untersuchungen am Kupferschiefer in Nordwestdeutschland;ein Beitrag zur Deutung der Genese bituminöser Sedimente. Geochimica et Cosmochimica Acta 28, 305 - 364.

Wedepohl, K.H., 1971. "Kupferschiefer" as a prototype of syngenetic sediment ore deposit. Society of Mining Geologists, Special Issue 3, 268 – 273.

Westermann, S., Vance, D., Cameron, V., Archer, C., Robinson, S.A., 2014. Heterogeneous oxygenation states in the Atlantic and Tethys oceans during Oceanic Anoxic Event 2. Earth and Planetary Science Letters 404, 178 – 189.

Wignall, P.B., 1994. Black Shales. Clarendon Press, Oxford. 127 pp.

Ziegler, P.A., 1990. Geological Atlas of Western and Central Europe. Shell International Petrology. Maatschappi B.V. Geological Society Publishing House, Bath, p. 1 – 239.

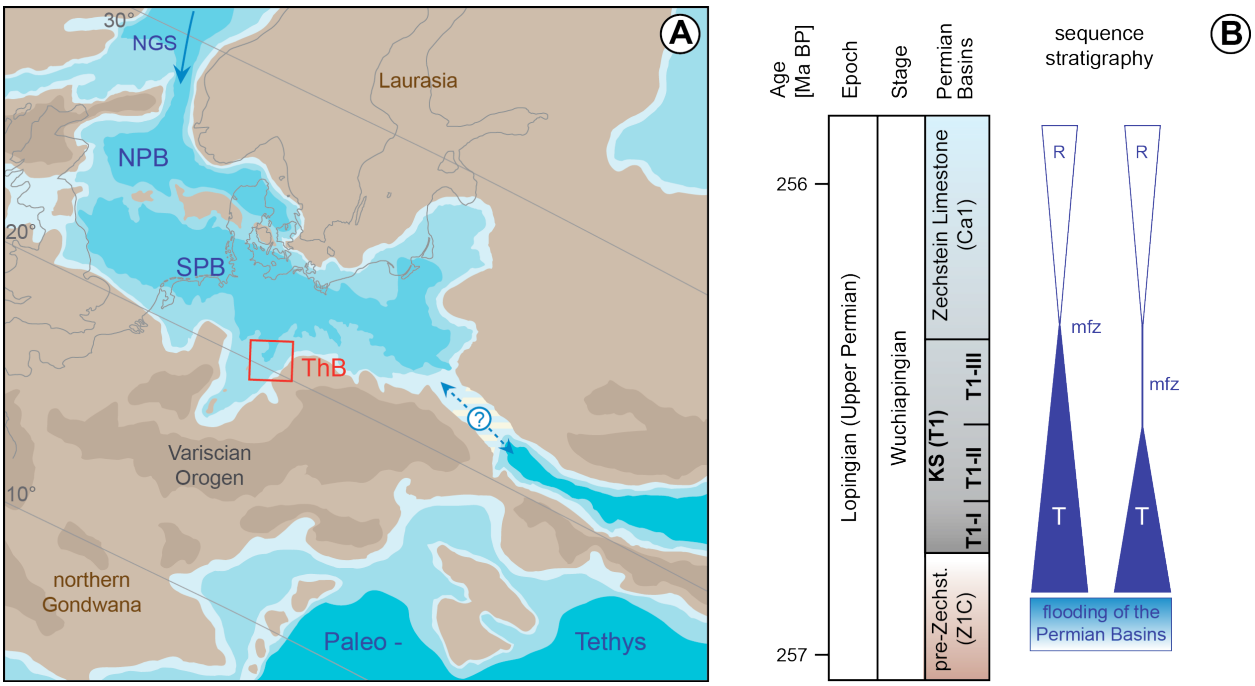

Fig. 1: A) Paleogeography of the European Permian Basins flooded during the Zechstein ingression. The Kupferschiefer (T1) was deposited in the Southern Permian Basin (SPB). The position of the Thuringian Basin (ThB) is shown in red. Paleogeography modified from Ziegler (1990) and Peryt et al. (2010) (NPB: Northern Permian; NGS: Norwegian-Greenland Sea). **B)** The Kupferschiefer is of Wuchiapingian (Upper Permian) age (e.g. Stollhofen et al., 2008; Schurlies, 2013; Ogg et al., 2016) and has been deposited during a rapid transgression. The maximum flooding zone (mfz) can be either placed in the Ca1 or in the upper T1 (nomenclature of lithological units after Strohmenger et al. (1996) and references therein). The Kupferschiefer sub-units (T1-I, T1-II, T1-III) have been distinguished based on sedimentological and geochemical parameters (Grice et al., 1996; Paul, 2006 and references therein; Fig. S1 in the supplementary information (SI)).

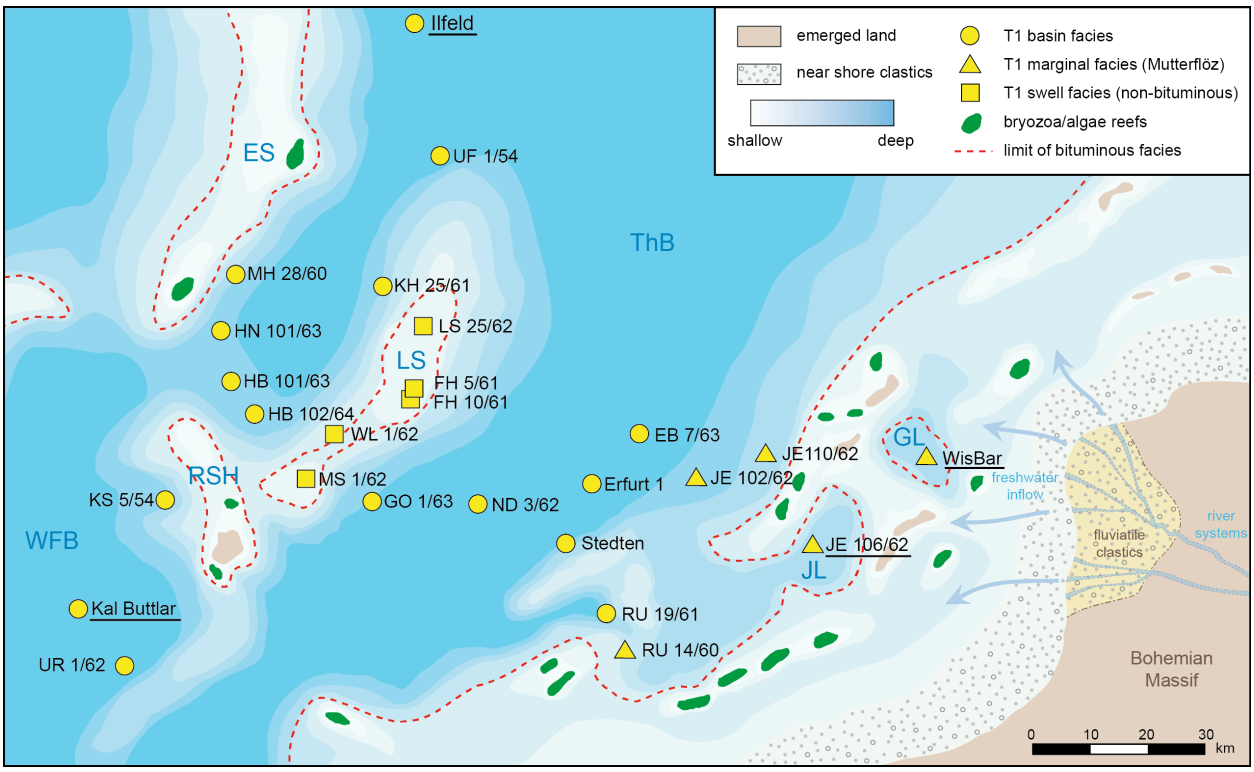

Fig. 2: Paleogeographic reconstruction of the Thuringian Basin during Kupferschiefer deposition. The eastern part of the basin represented a shallow lagoon environment in proximity to the paleo-coast line. Reef belts running parallel to the coastline possibly restricted the water exchange between the lagoon and the central Thuringian Basin. Information used in the paleogeographic reconstruction is provided in the SI. Symbols mark the position of Kupferschiefer profiles studied. All profiles have been analyzed for their OM and trace element content. Profiles underlined have been further subjected to $\delta^{98/95}$Mo and biomarker analysis. (ThB: Thuringian Basin, WFB: Werra-Fulda Basin, GL: Gera Lagoon; JL: Jena Lagoon; ES: Eichsfeld Swell; LS: Langensalza Swell; RSH: Ruhla-Schmalkalden High).

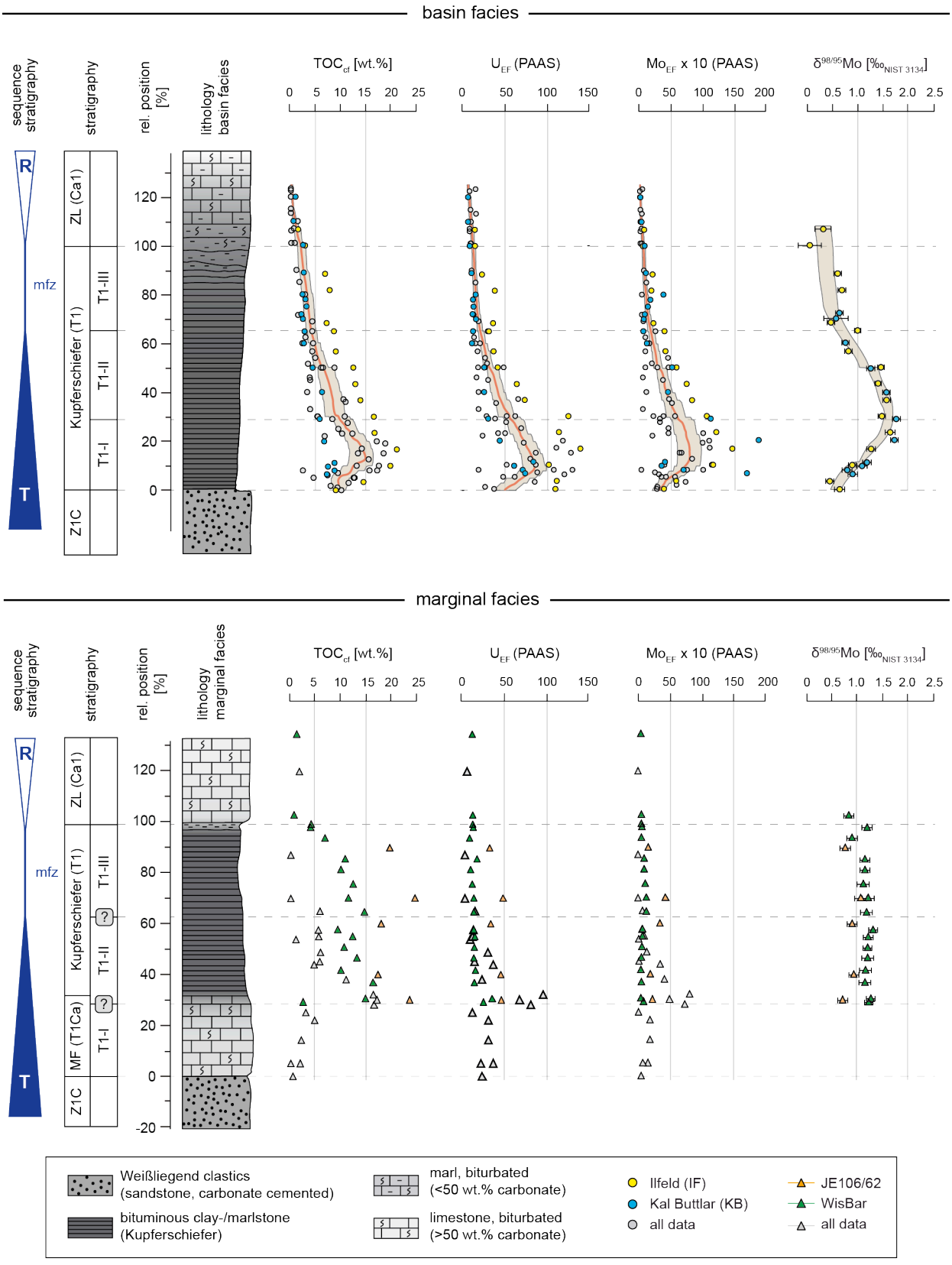
basin facies
sequence stratigraphy
stratigraphy
rel. position [%]
lithology basin facies
TOC$_{cf}$ [wt.%]
U$_{EF}$ (PAAS)
Mo$_{EF}$ x 10 (PAAS)
δ$^{98/95}$Mo [‰$_{NIST\ 3134}$]
R
mfz
T
ZL (Ca1)
Kupferschiefer (T1)
T1-III
T1-II
T1-I
Z1C
marginal facies
MF (T1Ca)
Weißliegend clastics (sandstone, carbonate cemented)
bituminous clay-/marlstone (Kupferschiefer)
marl, biturbated (<50 wt.% carbonate)
limestone, biturbated (>50 wt.% carbonate)
Ilfeld (IF)
Kal Buttlar (KB)
all data
JE106/62
WisBar
all data

Fig. 3: Stratigraphic trends (including kernel regressions with 95% confidence intervals) for TOC_{cf} content, U_{EF}, Mo_{EF} and $\delta^{98/95}Mo_{SED}$ for basinal (top) and marginal settings (bottom). Comparable trends in TOC_{cf}, U_{EF} and Mo_{EF} occurred in basin settings, whereas more variable trends between marginal sites indicated a greater importance of local controls on OM and RSTE enrichment. Overall low TOC_{cf} as well as low U_{EF} and Mo_{EF} without any stratigraphic trends were determined at swell settings (Z1C: Weissliegend clastics; MF (T1Ca): Mutterflöz; ZL (Ca1): Zechstein Limestone).

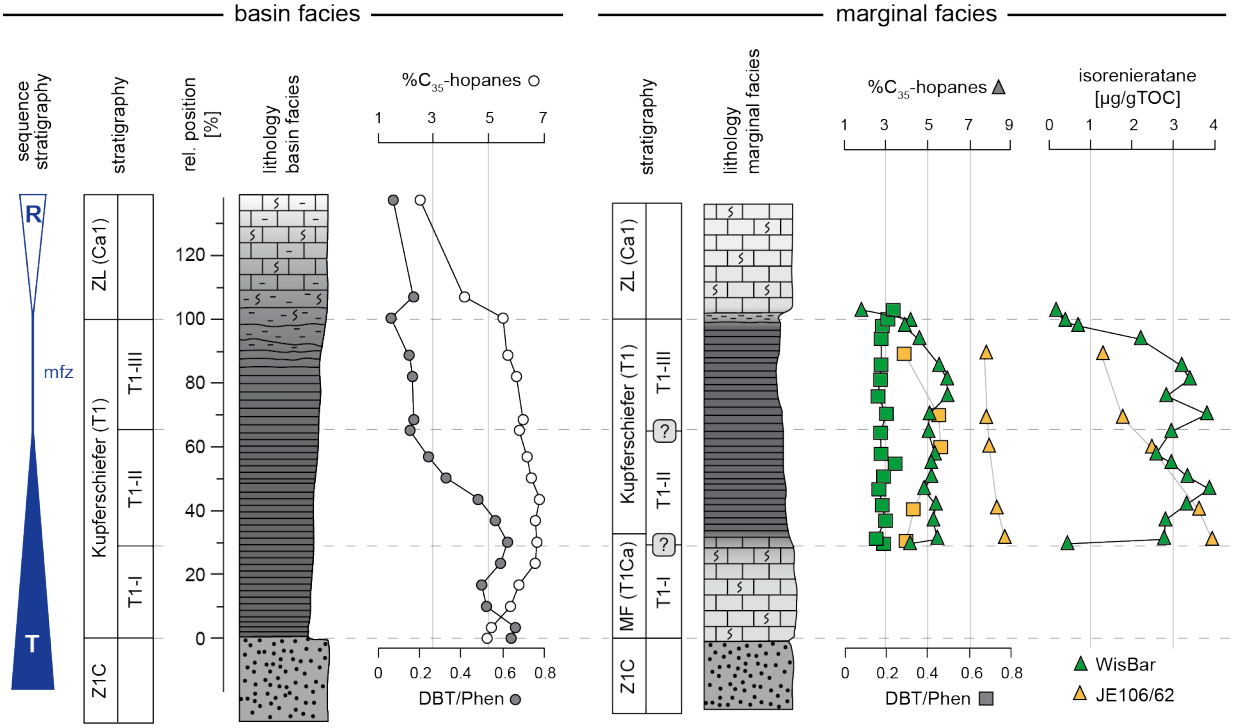

Fig. 4: Stratigraphic trends for selected redox-sensitive bio-/geomarker proxies for the basin setting at Ilfeld and for the marginal settings WisBar and JE106/62. The redox-sensitive preservation of C_{35} hopanes is expressed as a percentage, whereas the degree of sulfur-incorporation into OM can be inferred from the DBT/Phen ratio. The presence of isorenieratane in samples from cores JE106/62 and WisBar indicated euxinic conditions extending from bottom waters into the photic zone.

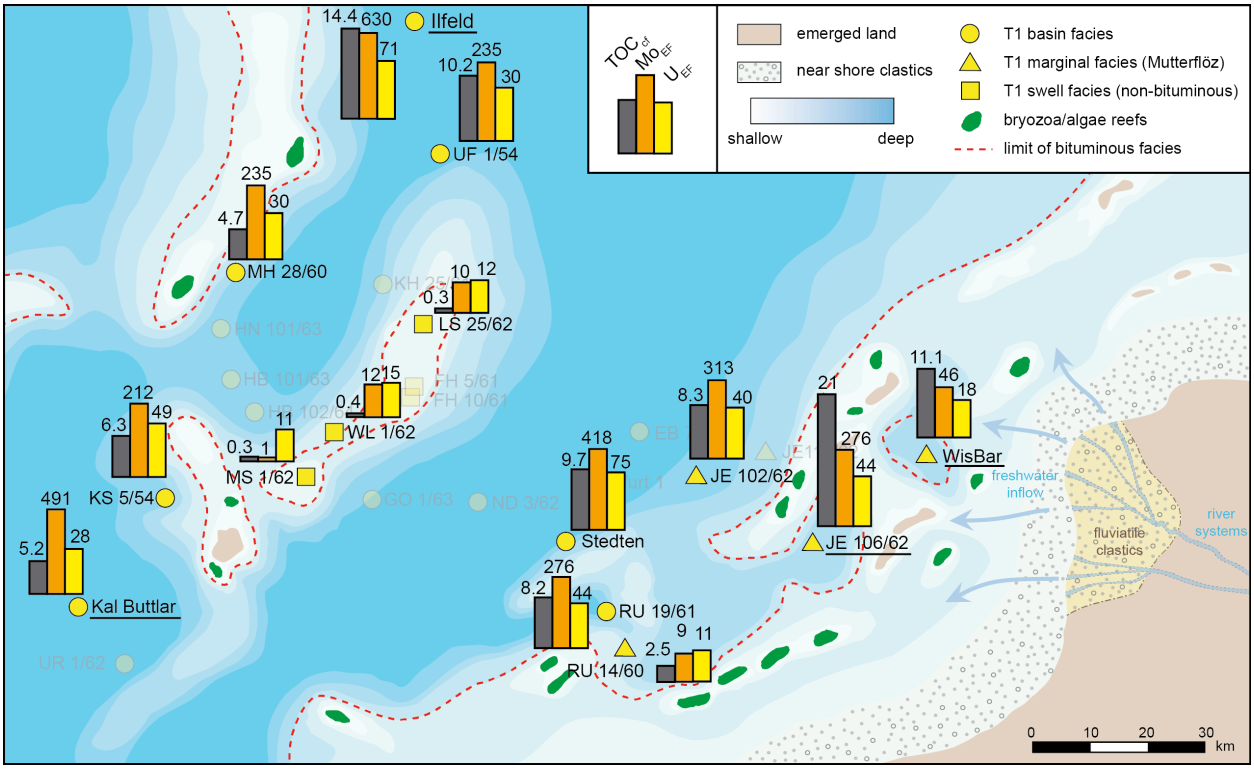

Fig. 5: Spatial variations in the enrichment pattern of U, Mo and TOC_{cf} in the different Kupferschiefer facies types (basin, marginal, swell) that could be associated with contrasting depositional environments. Data shown here are average values for complete T1 profiles (TOC_{cf} values plotted on a linear, Mo_{EF} and U_{EF} on a logarithmic scale). At basin settings euxinic conditions were indicated by high Mo_{EF} and by high TOC_{cf} values. Low U_{EF}, Mo_{EF} and TOC_{cf} values at swell settings reflect preferentially suboxic/oxic conditions. A higher degree of variability in enrichment patterns at marginal settings highlighted the role of local oceanographic conditions in controlling the redox regime.

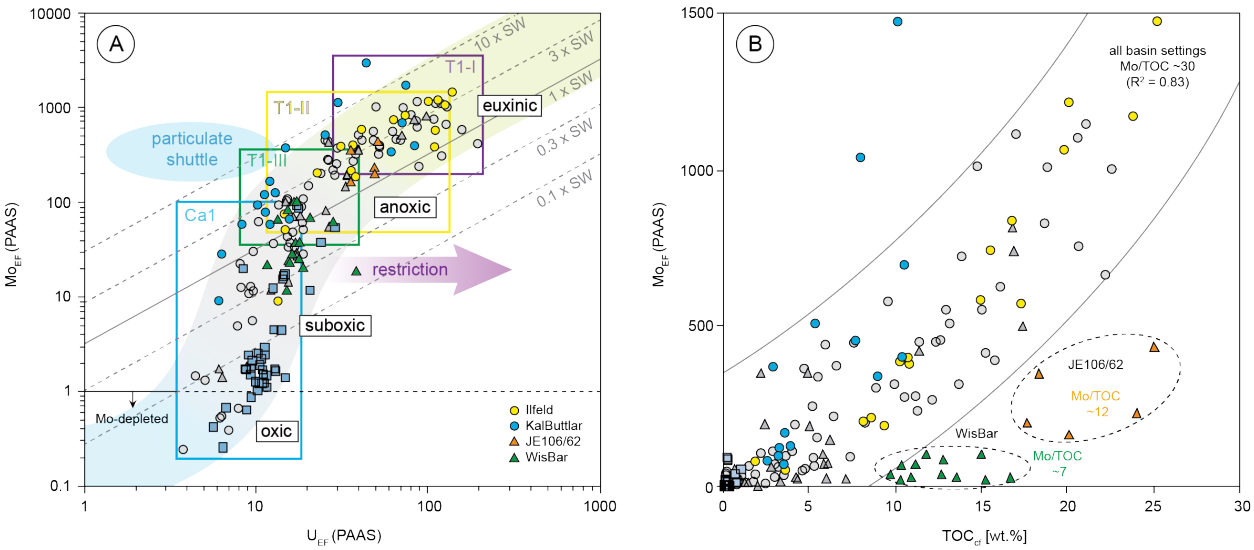

Fig. 6: A) Mo_{EF} versus U_{EF} for the different Kupferschiefer facies types (symbols as defined in Fig. 2). Data ranges for samples from the T1-I, T1-II and T1-III sub-units, distinguished at basin settings, are indicated by boxes. All samples plotted along an open marine, unrestricted trend (Algeo &Tribovillard, 2009), with highest Mo_{EF} and U_{EF} for samples at basin settings during T1-I and T1-II times. Seawater Mo/U ratios given here are for present-day seawater (3.1 when expressed as sedimentary abundance ratio, corresponding to molar ratio of ~7.7). **B)** Plot of TOC_{cf} versus Mo_{EF} confirming that Mo-enrichment in the Kupferschiefer was associated with elevated organic matter enrichment. Mo/TOC ratios of ~30 indicated weak hydrologic restriction, when assuming present day Mo/TOC patterns (Algeo & Lyons, 2006; Algeo & Rowe, 2012). Lower Mo/TOC ratios of ~12 and ~7 noted at sites JE106/62 and WisBar, respectively, pointed to a stronger hydrological restriction at these sites, resulting in a depletion of aqueous Mo. Mo/TOC ratios were calculated on the base of raw data.

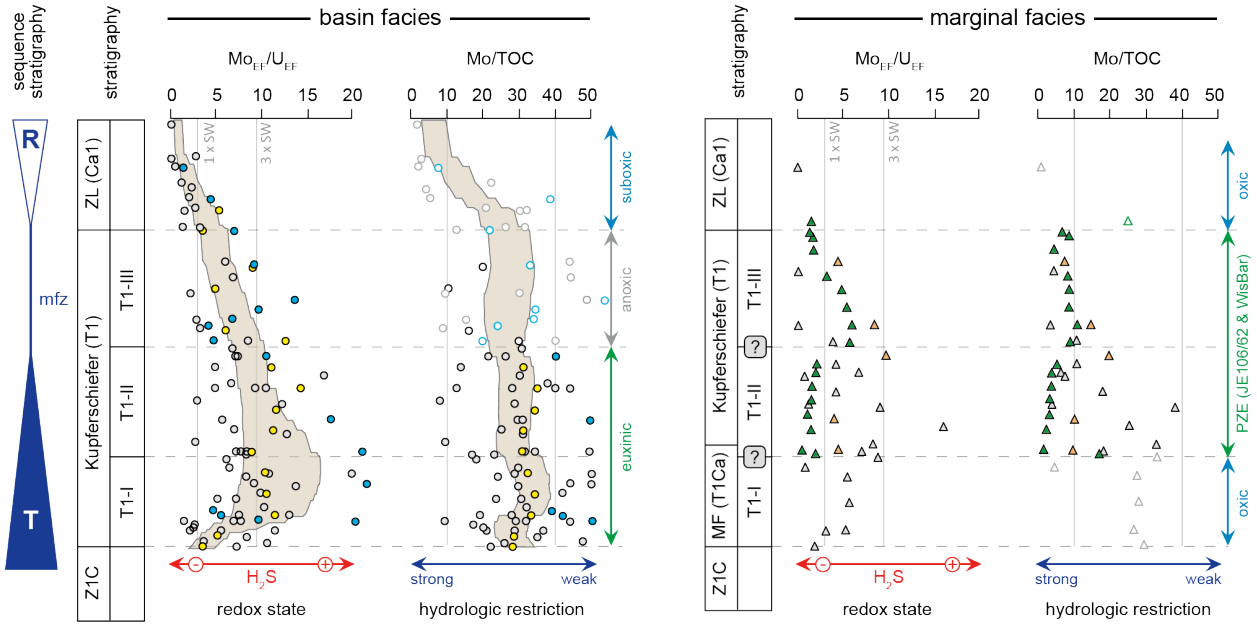

Fig. 7: Stratigraphic evolution of Mo_{EF}/U_{EF} and Mo/TOC ratios for basin and marginal settings. High Mo_{EF}/U_{EF} ratios during T1-I and T1-II times in basin settings attested to the presence of euxinic water masses overlying the sediment. During these times Mo-replete waters could be inferred from high Mo/TOC ratios and attested to weak hydrologic restriction (tends indicated by kernel regressions with 95% confidence intervals). More pronounced Mo-depletion at sites JE106/62 and WisBar were indicated by low Mo/TOC ratios. Note that the Mo/TOC ratio is a proxy for water mass restriction only under euxinic conditions (see Algeo & Lyons, 2006). Open symbols in the Mo/TOC plots are for samples deposited under oxic-anoxic conditions (otherwise symbols as defined in figure 3).

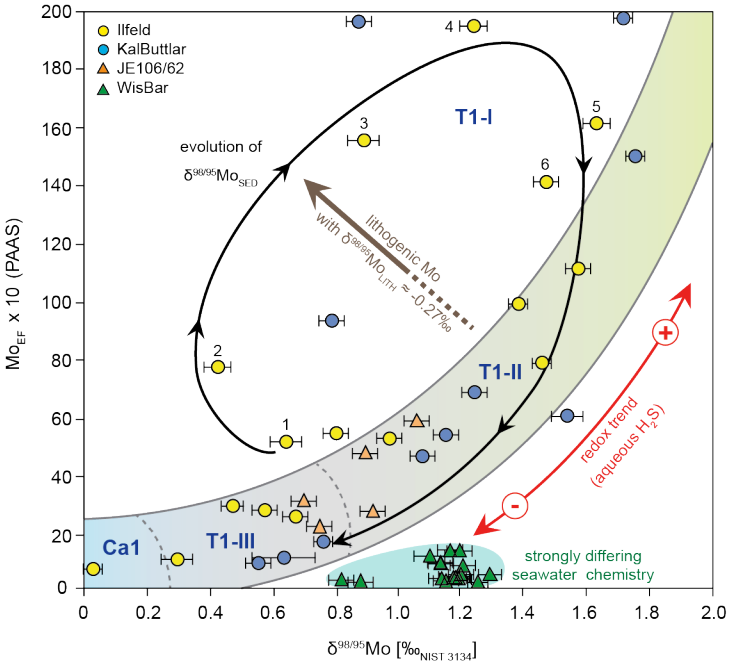

Fig. 8: Binary diagram of $\delta^{98/95}Mo_{SED}$ values versus Mo_{EF}. Most samples plotted along a trend reflecting redox-dependent variation in Mo uptake and isotopic fractionation. Samples from the T1-I sub-unit as well as from core WisBar deviated from this trend, which points to additional mechanisms impacting on Mo accumulation and $\delta^{98/95}Mo_{SED}$. See text for discussion.

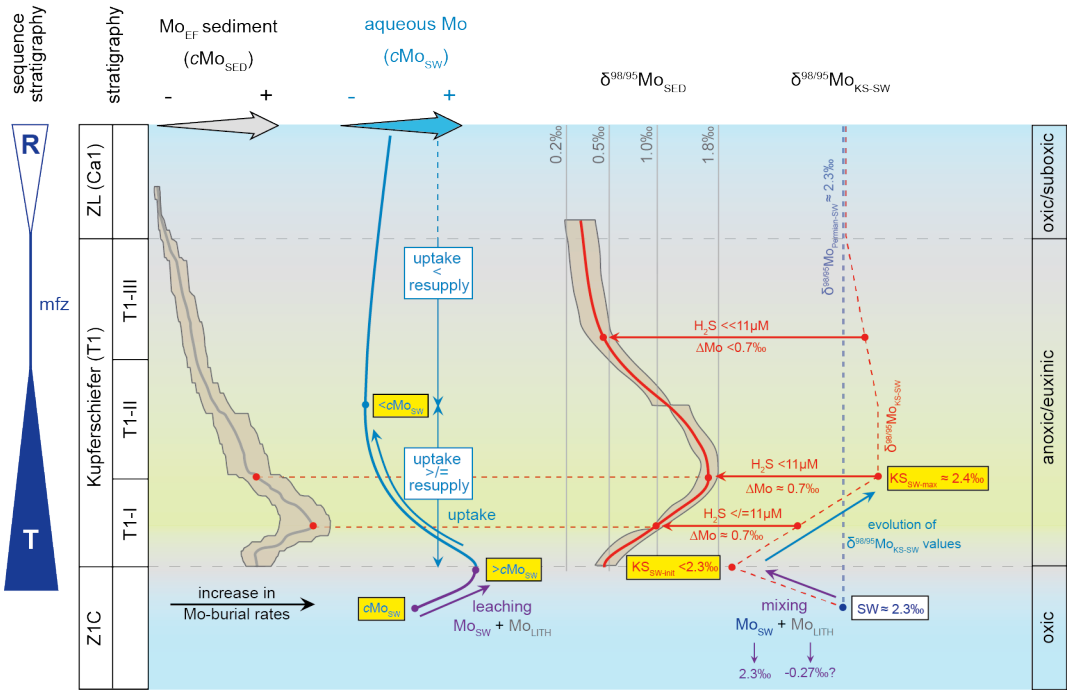

Fig. 9: Model illustrating the evolution of aqueous and sedimentary Mo abundance and isotopic composition. See text for discussion (cMo_{SW}: aqueous Mo concentration; Mo_{SW}: Mo in open ocean seawater; Mo_{LITH}: lithogenic Mo).

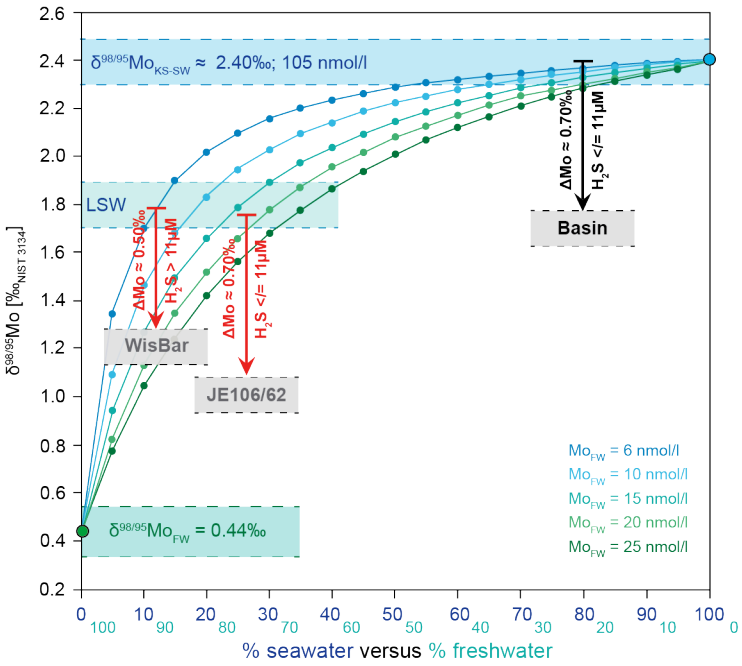

Fig. 10: Two-component mixing model to illustrate the effect of mixing variable percentage of Mo-depleted fluvial freshwater (Mo_{FW} = variable; $\delta^{98/95}Mo_{FW}$ = 0.44‰ (Archer & Vance, 2008)) with marine water ($Mo_{KS\text{-}SW}$ = 105 nmol/l; $\delta^{98/95}Mo_{KS\text{-}SW}$ = 2.40‰) in the lagoon setting (LSW: lagoon seawater).

A T1-I

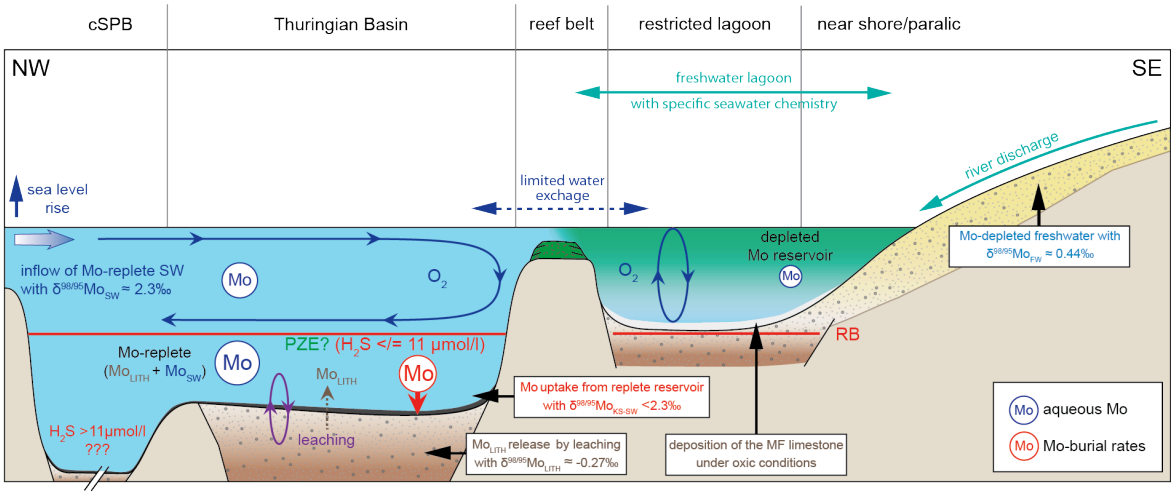

B lower T1-II

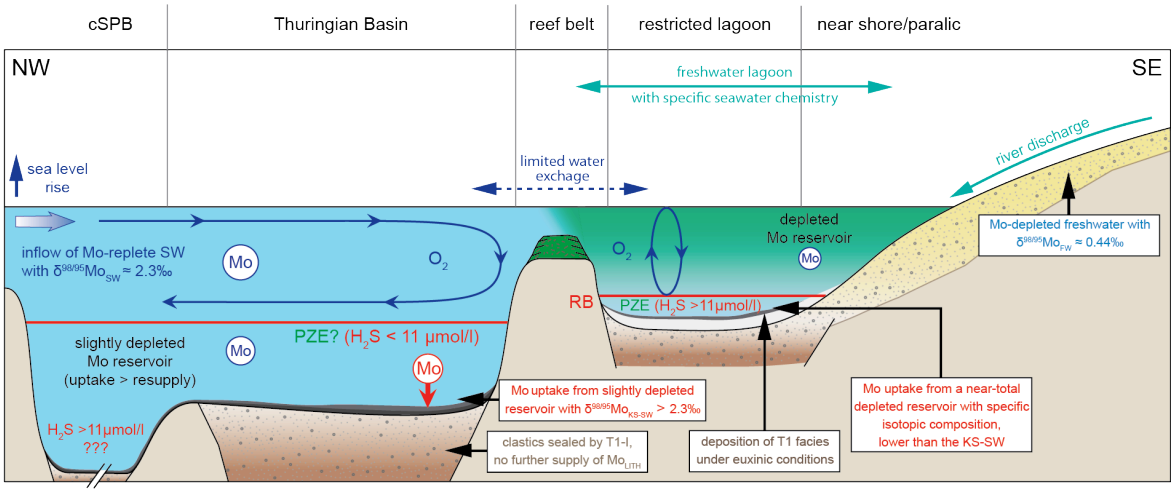

C upperT1-II & T1-III

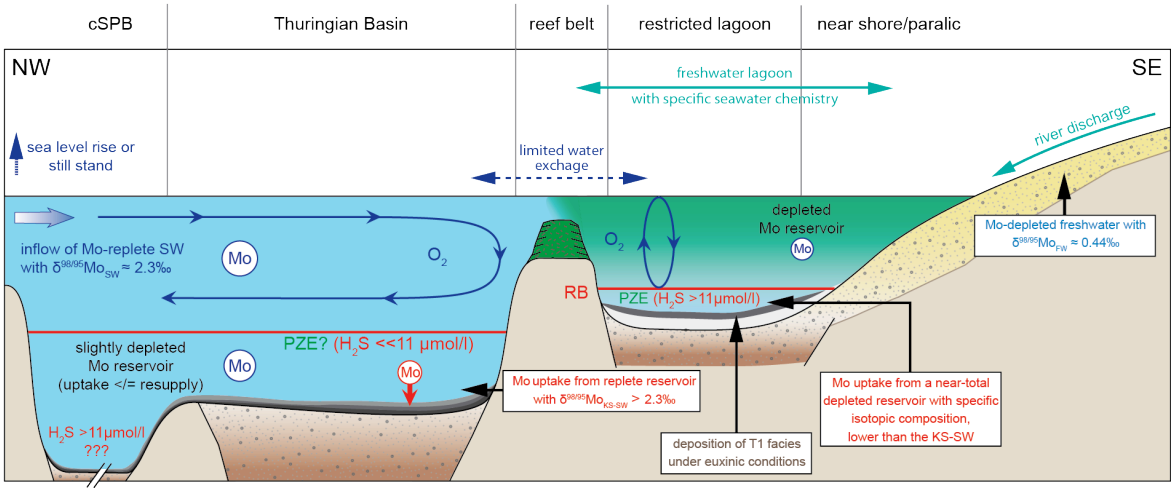

Fig. 11: Simplified schematic depositional model for the Kupferschiefer from the Thuringian Basin (the cross section is not to scale, the central Southern Permian Basin (cSPB) covered a much wider area than the Thuringian Basin, compare with Fig. 1a). Redox conditions varied temporally and spatially and were controlled by paleogeography and sea level evolution. At restricted marginal sites the seawater chemistry (RSTE inventory and Mo-isotope composition) was affected by riverine freshwater supply. Moreover, leaching of pre-existing strata and release of RSTE impacted on the seawater chemistry at basinal sites during early T1-I times. The levels of aqueous Mo concentration and Mo burial rates are given by size of blue and red circles, respectively. See text for detailed discussion (PZE: photic zone euxinia).

Table. 1: Geochemical data for the samples investigated. Shown are average values and data ranges for the Kupferschiefer (T1) sub-units (n.a. = not analyzed; AI = aryl isoprenoids; Isor. = isorenieratane; + present; ++ present at high abundance; - not present). Molecular geochemical investigations of samples from the Mutterflöz and from swell settings were prohibited by the low OM content.

	proxy / sub-unit	TOC_{cf} [wt.%]	U_{EF}	Mo_{EF}	Mo_{EF}/U_{EF}	Mo/TOC	$\delta^{98/95}Mo$ [‰$_{NIST\ 3134}$]	C_{35} hop. [%]	DBT/Phen	*Chlorobi* lipids
basin	Ca1	0.7 0.2 - 1.9	10 6 - 17	19 1 - 76	2 0 - 5	18 9 - 39	0.3	3.4 2.6 - 4.1	0.1 0.1 - 0.2	AI: + Isor.: -
basin	T1-III	4.5 1.6 - 10.5	18 8 - 38	135 34 - 390	8 2 - 25	28 8 - 65	0.6 0.03 - 0.98	5.7 5.5 - 6.0	0.1 0.1 - 0.2	AI: + Isor.: -
basin	T1-II	8.6 3.0 - 19.8	37 11 - 125	368 48 - 1056	10 3 - 20	28 9 - 133	1.3 0.76 - 1.76	6.5 6.2 - 6.9	0.4 0.2 - 0.6	AI: + Isor.: -
basin	T1-I	14.1 3.1 - 23.8	82 24 - 193	641 199 - 1460	9 5 - 37	32 2 - 118	1.1 0.43 - 1.73	5.9 4.9 - 6.7	0.6 0.5 - 0.7	AI: + Isor.: -
margin	Ca1	1.5 1 -2.1	13 9 - 15	13 2 - 24	1 0 - 2	12 1 - 25	0.8	1.5 1.2 - 1.8	0.2	AI: + Isor.: -
margin	T1 (s.l.)	11.2 0.4 - 25	29 6 - 98	157 1 - 813	4 1 - 16	11 2 - 38	1.1 0.70 - 1.30	5.8 3.1 - 8.7	0.2 0.2 - 0.5	AI: ++ Isor.: ++
margin	T1Ca	1.5 0.3 - 2.9	31 25 - 39	135 55 - 211	4 2 - 6	41 17 - 81	n.a.	n.a.	n.a.	n.a.
swell	not sub-devided	0.7 0.1 - 1.1	12 6 - 29	10 0.3 - 90	0.6 0 - 5	20 1 - 69	n.a.	n.a.	n.a.	n.a.